



**Politecnico
di Torino**

Politecnico di Torino

Master of Science in Civil Engineering

Master Thesis

***Dynamic Analysis of Crack Growth Using Sub-Parametric eXtended
Finite Element Method***

**Supervisor:
Prof. Giulio Ventura**

**Candidate:
Vida Bagherpour Aliabadi**

November 2023

Acknowledgements

I wish to convey my gratitude to my esteemed supervisor, Professor Giulio Ventura, for his exceptional guidance and unwavering support. His expertise and mentorship have not only enriched this thesis but also nurtured my academic growth.

To my beloved family, I owe a debt of immense gratitude. Your constant love, enduring encouragement, and unwavering understanding have been the cornerstone of my success. I feel truly blessed to have your support.

Abstract

This thesis presents a comprehensive study on the dynamic analysis of crack growth, with a focus on improving the accuracy of predicting stress intensity factors, crack tip velocity, and related parameters. It introduces some strategies to appropriately model crack propagation under dynamic loading conditions and mitigate numerical oscillations that commonly affect computational results.

In the pursuit of more precise time integration methods, the study employs the Discontinuous Galerkin method, which proves to be superior to traditional approaches like the Newmark method. This choice is justified by the Discontinuous Galerkin method's ability to handle discontinuities in variables over time, aligning with the dynamic nature of crack growth analysis.

As cracks extend, they generate residual forces that can destabilize numerical solutions. To address this issue, a balance recovery algorithm is implemented, effectively eliminating such forces and enhancing solution stability.

The research also showcases the efficacy of an interaction integral method for calculating stress intensity factors. A series of practical examples is solved to demonstrate the method's utility in predicting crucial parameters related to crack growth.

In scenarios involving non-uniform meshes, the thesis proposes a sub-parametric element approach. This approach utilizes 3-node elements for geometry discretization and 4-node elements for other field variables, ensuring a constant Jacobian matrix within each element. The application of this method serves to minimize errors in solution outcomes, particularly in situations where the mesh is non-uniform.

Overall, this thesis offers a comprehensive framework for dynamic crack growth analysis, combining advanced numerical techniques with innovative strategies to enhance the accuracy and reliability of predictions in the field of fracture mechanics.

Keywords: *extended finite element method, dynamic analysis, fracture mechanics, sub-parametric element.*

Contents

1	Introduction.....	7
1.1	Dynamic fracture mechanics.....	7
1.2	eXtended Finite Element Method	10
2	Extended Finite Element Method	26
2.1	General Principles of the Method	27
2.2	Crack Modelling.....	29
2.2.1	Modeling Crack Surfaces and Heaviside Enrichment Function	29
2.2.2	Modeling Crack Tip and Enrichment Functions	33
2.3	The implementation of the extended finite element method.....	36
2.3.1	Formation of Matrices	37
2.4	Methods of Spatial Integration.....	39
2.5	Temporal Integration of the Dynamic Equilibrium Equation	41
2.6	Balance Recovery During Crack Growth	48
2.7	Calculating fracture parameters using the interaction integration (<i>Md</i>)	50
2.8	Dynamic Fracture Criterion	55
2.9	Sub-parametric element	56
3	Examples.....	60
3.1	An Edge Crack in a Finite Plate	60
3.2	Tensile Plate with a Central Inclined Crack	63
3.3	Stationary mixed mode crack.....	63
3.4	Stationary and Moving Crack in Mode I.....	66
4	Conclusion and Suggestions	78
4.1	Conclusion.....	78
4.2	Suggestions.....	79
5	References.....	80

Figure 1- The influence domain for node J, when the node is positioned on the lateral face of the elements (Mohammadi, 2008).	29
Figure 2-Heaviside function as $H\xi$	31
Figure 3-Enriched shape functions for nodes 2 and 3 and application of the shifting Heaviside function.	31
Figure 4- The local coordinates of the crack tip and the vectors that are normal and tangential to the extended Heaviside function at a point like xI , which is the nearest point on the crack to the point x	32
Figure 5- The selection of nodes for enrichment involves choosing nodes that are indicated by circles for enrichment with the extended Heaviside function and nodes that are indicated by squares for enrichment with functions near the crack tip (Mohammadi, 2008).	33
Figure 6 The enrichment functions near the crack tip, when the crack is positioned at the center of the parent element and the angle between the crack faces and the horizontal axis is $\pi/8$ (Mohammadi, 2008).	36
Figure 7- Determining $A +$ and $A -$ for node J is discussed in reference(Mohammadi, 2012).	37
Figure 8- The subdivision of elements involved with cracks into sub-triangles for the purpose of integration (Mohammadi, 2012).	40
Figure 9- The Heaviside function's effect on the time-dependent shape functions	45
Figure 10- To maintain equilibrium during the mapping of degrees of freedom to the new configuration.	49
Figure 11- The paths and the enclosed surfaces associated with the J-integral(Mohammadi, 2012).	52
Figure 12- The nodal values of the q function in a regular finite element mesh, where $q=1$ is represented in blue and $q=0$ in green, are shown in the diagram.	53
Figure 13-Geometry of the tensile plate with an edge crack(a), the finite element mesh, and the M-integral domain.	61
Figure 14- stress contours on the deformed shape of the plate a) σ_{xx} , b) σ_{yy} , c) σ_{xy} .	62
Figure 15- Geometry and the mesh for the mixed mode central crack problem.	63
Figure 16-Geometry and Loading	64

Figure 17-Normalized SIF plotted against normalized time for a stationary semi-infinite mixed-mode crack.....	65
Figure 18-The geometry and boundary conditions for the discussed example	67
Figure 19- The dynamic stress intensity factor for the recommended mesh in the reference (Liu et al., 2011).	70
Figure 20- The analysis conducted in the study involved two different time integration methods: the discontinuous Galerkin time integration and the Newmark method.	71
Figure 21- The inclusion of the balance-recovery algorithm along with the Discontinuous Galerkin (Edgerton & Barstow) time integration method has a significant impact on the numerical simulations.	71
Figure 22- The influence of the balance recovery algorithm in conjunction with the Newmark integration method.	72
Figure 23- The Effect of Mesh Refinement in the Horizontal Direction.....	73
Figure 24-The Effect of Mesh Refinement in the Vertical Direction	73
Figure 25- Comparison of Mesh Refinement with Equal Division in Horizontal and Vertical Directions	74
Figure 26- Comparison of Different Time Steps.	75
Figure 27- Comparison of Various Radii for the Md Integral	75
Figure 28- A snapshot of the non-uniform mesh utilized in this example.....	76
Figure 29- A comparison of the Stress Intensity Factors with the uniform and non-uniform meshes.....	77
Figure 30- A comparison of the Stress Intensity Factors with sub-parametric and iso-parametric elements.....	77

Table 1-Evaluating XFEM predictions for stress intensity factor against the analytical solution across various crack sizes.	60
Table 2-Evaluating the normalized mode I and II stress intensity factors against the analytical solution across various crack angles.	64
Table 3- Material properties.....	65
Table 4- Material properties.....	66

1 Introduction

1.1 Dynamic fracture mechanics

Dynamic fracture mechanics is a highly specialized discipline within fracture mechanics that focuses on the behavior of materials and structures when subjected to rapid and time-dependent loading conditions. This field is particularly concerned with understanding how cracks and fractures propagate under the influence of high-speed or dynamic forces, such as those encountered in explosions, impacts, or fast-moving objects.

The central objective in dynamic fracture mechanics is the analysis of crack propagation. Researchers delve deep into the mechanisms of crack initiation, growth, and arrest under dynamic loading conditions. What sets this apart from static fracture mechanics is the influence of inertia. Rapidly changing loads introduce inertia effects that significantly impact the dynamics of crack propagation. The presence of material inertia results in the propagation of loads in the form of stress waves. As a crack advances, it creates new free boundaries. The interaction between these stress waves and the advancing crack makes dynamic fracture problems significantly more complex than static crack scenarios. For instance, when applying a static tension load parallel to the crack direction, there is no concentration of force at the crack tip location. However, introducing a tension stress impulse wave in the same direction will lead to the initiation of a mode I crack as it propagates to the tip location. This occurs due to transverse inertial effects.

The concept of the energy release rate, which quantifies the energy required for a crack to propagate, is fundamental in dynamic fracture analysis. It serves as a critical parameter for predicting whether a crack will propagate or arrest under the extreme conditions of dynamic loading. This concept allows for precise calculations and predictions in highly dynamic environments.

Furthermore, the dynamic material fracture toughness is closely tied to the loading rate. This added dependency on loading rate makes the analysis and experimentation of dynamic fracture problems more challenging. The difficulties stem from the presence of high stress gradients, variations in loading stress wave forms, and the rapid propagation of cracks at the crack tip location.

The earliest empirical investigations into dynamic fracture likely revolved around incidents such as the bursting of military cannon or the impact loading of industrial machinery in the 19th century (Freund, 1990; Kirkaldy, 1863).

During the early days of fracture mechanics, it was generally assumed that a structure would experience total failure when a crack became unstable and initiated growth (Tipper, 1962). Consequently, the phase of rapid crack growth was explored primarily out of curiosity by a limited number of researchers, without significant practical implications. Nevertheless, in the 1970s, there was a growing realization of the importance of comprehending crack propagation, crack arrest, and dynamic effects in engineering applications and earth sciences, which led to substantial and continuous progress in this field (Freund, 1990).

Dynamic fracture mechanics, broadly categorized into stationary and propagating cracks, represents a pivotal aspect of classical fracture mechanics, particularly in scenarios where the influence of material inertia and strain rate-dependent material properties plays a substantial role in studying the stability and progression of existing cracks (Freund, 1990).

Inertia effects can emerge from dynamic loads applied to a cracked solid or from the rapid propagation of a crack. When dynamic loading is imposed on a cracked solid, the stress waves generated affect all parts of the material, including the pre-existing crack. The transient force acting on the crack dictates whether it remains stationary or propagates. The interaction between the rapid motion of the crack and the stress wave field radiated from a moving crack holds significance in various material testing techniques and several vital engineering applications, such as seismology (Freund, 1990).

In the context of brittle fracture in elastic solids, cracks can propagate at velocities significant enough to markedly influence the stress and displacement fields through elastodynamic effects (Achenbach & Bazant, 1975). Nonetheless, dynamic effects may not be universally significant in every fracture problem. For instance, when the characteristic loading time is short compared to the time needed for a stress wave to travel over the length of the crack or the distance from the crack edge to the loaded boundary, it can be anticipated that inertia effects will be inconsequential. In contrast, when the speed of the crack tip or

edge constitutes a substantial fraction of the lowest characteristic wave speed of the material, dynamic effects must be taken into account (Freund, 1990).

Despite extensive research efforts, certain issues within the field of dynamic fracture remain contested. These include topics like the terminal speed of cracks or the bifurcation of dynamic cracks under symmetric tensile loading. There is also a puzzling observation that running cracks appear to have a maximum speed determined by the material itself rather than the loading or geometric configuration (Edgerton & Barstow, 1941).

When it comes to studying dynamic fracture phenomena, whether through experimentation, analysis, or numerical simulations, the challenges are considerable compared to their static counterparts due to the time-dependent nature of all contributing parameters.

In dynamic fracture experiments, specialized data loggers capable of recording accurate sequential measurements in a very short timeframe are essential. These tests become even more intricate when studying crack growth, as data must be gathered in the same brief period when changes are occurring. Since the late 1940s, optical methods of observation and high-speed photography techniques have been developed to study the behavior of propagating cracks. These methods include the optical shadow spot method, introduced by (Manogg, 1966), which allows for the direct inference of the instantaneous crack-tip stress intensity factor and crack-tip position. Other techniques include the multiple spark arrangement devised by (Wells, 1958) and the superimposed ultrasonic technique developed by (Kerkhof, 1973). The latter technique illustrates that the crack tip itself lacks effective inertia and that a brittle crack subjected to oblique incident stress waves can gradually curve toward the local direction of maximum tensile stress. For more information on earlier experimental work regarding the effects of stress waves on fractures in brittle materials, one can refer to reviews by (Dally, 1987; Freund, 1990; Kalthoff, 1987)

The time-dependent nature of dynamic fracture processes necessitates the application of complex analytical approaches founded on intricate mathematical formulations. (Yoffe et al., 1951), (Craggs & Solids, 1960), and (Baker, 1962) demonstrated that the maximum stress field values near a propagating crack tip shift out of the plane of crack propagation when the speed of the crack tip surpasses a certain critical threshold.

(J. R. Rice, 1968; J. R. J. F. a. a. t. Rice, 1968) conducted analyses of steady-state elasto-dynamic problems to explore the general characteristics of near-tip stress fields in isotropic materials, utilizing complex-variable techniques. (Achenbach, 1972), (Freund & Clifton, 1974), and (Achenbach & Bazant, 1975) developed analytical methods for assessing elasto-dynamic stress fields in the vicinity of propagating cracks. These methods were based on the initial work by (Cotterell, 1964) and drew upon mathematical models by (Williams, 1952). Their research revealed that the steady-state solution also holds validity for transient cracks in the near-tip region.

Efforts akin to those by (Freund & Clifton, 1974) and (Freund, 1976) were dedicated to exploring non-uniform crack propagation. Additionally, (Nilsson, 1974) delved into the angle dependence of near-tip fields, while (Chen, 1978) investigated the stress and displacement fields in dynamic stationary crack problems. (Nishioka & Atluri, 1983, 1984) and (Freund, 1990) examined the dynamics of crack propagation at high speeds, contributing to the body of knowledge in this area.

1.2 eXtended Finite Element Method

The finite element method stands out as one of the most widely used numerical techniques for approximating solutions to partial differential equations. It has been successfully applied across various fields within the realm of engineering, including aeronautical and aerospace engineering, the automotive industry, mechanical engineering, civil engineering, biomechanics, geomechanics, material sciences, and more.

Nevertheless, despite its widespread use, the FEM does come with certain limitations. There are situations where it poses constraints on its efficient application. The FEM relies on the approximation characteristics of polynomials, often necessitating smooth solutions to achieve optimal accuracy. In cases where the solution exhibits non-smooth behavior, such as high gradients or singularities in the stress and strain fields or strong discontinuities in the displacement field, as seen in the context of cracked bodies, the FEM becomes computationally expensive to achieve optimal convergence.

In the context of the Finite Element Method, handling non-smooth displacements near the crack tip typically involves local mesh refinement. However, this can lead to a significant increase in the number of degrees of freedom, especially in three-dimensional scenarios. Additionally, the incremental computation of crack growth necessitates frequent remeshing, which not only incurs a substantial computational cost but also may negatively impact result quality. The classical FEM has shown limitations in its ability to effectively address fracture mechanics problems.

To address these computational challenges, an innovative approach involves leveraging prior knowledge of the exact solution. An early concept was to apply the asymptotic crack tip displacement solution to the finite element basis. A significant advancement in crack modeling emerged with the development of a Partition of Unity (Melenk et al., 1996) based enrichment method for discontinuous fields, referred to as the Extended Finite Element Method (X-FEM), as presented in Dolbow's PhD dissertation in 1999 (Dolbow, 1999).

In the X-FEM, special functions are introduced into the finite element approximation using the PU framework. For crack modeling, discontinuous functions like the Heaviside step function and two-dimensional linear elastic asymptotic crack tip displacement fields are employed to account for the presence of the crack. This approach allows modeling the domain with finite elements without explicit meshing of the crack surfaces. Notably, the location of the crack discontinuity can be arbitrary with respect to the underlying finite element mesh, and simulating crack propagation can be carried out without the need for remeshing as the crack advances. The X-FEM has especially demonstrated its potential in the field of fracture mechanics (Fries & Belytschko, 2010).

The foundational research articles on the Extended Finite Element Method were authored by (Belytschko & Black, 1999) and (Moës et al., 1999). Their work focused on elastic fracture propagation and introduced a groundbreaking concept known as "A FEM for crack growth without remeshing." In this approach, they devised a minimally remeshing Finite Element Method for simulating crack growth by incorporating discontinuous enrichment functions into the finite element approximation to account for the presence of the crack. The core concept revolved around the addition of enrichment functions to the approximation space, specifically within a space that accommodates a discontinuous

displacement field. Consequently, this method allowed cracks to be arbitrarily oriented within the mesh. It's worth noting that a similar set of functions had been previously developed by (Fleming et al., 1997) for enriching the Element-Free Galerkin method. This method capitalizes on the Partition of Unity (Melenk et al.) property of finite elements, a property that had been highlighted by (Melenk et al., 1996). This PU property essentially dictates that the sum of the shape functions must equal one. This property has long been recognized, as it corresponds to the capability of shape functions to accurately represent a constant value, which is essential for ensuring convergence in numerical analysis.

By allowing arbitrary functions to be locally integrated into the Finite Element Method (FEM) or mesh-free approximation, PUM offers flexibility in modeling moving discontinuities without altering the underlying mesh. Meanwhile, the set of enrichment functions evolves (or their supports change) in tandem with the interface geometry. In addition to easing the modeling of moving discontinuities, enrichment enhances the local approximation capabilities of the solution space by enabling the incorporation of arbitrary functions within the basis. This proves particularly valuable for problems characterized by singularities or boundary layers.

Both methods can be used with both structured and unstructured meshes. Structured meshes are valuable for materials science studies, where the goal is to determine the properties of a material's unit cell. On the other hand, unstructured meshes are often preferred for the analysis of engineering structures and components, where mesh conformity with external boundaries is desirable. Some emerging methods today can even handle complex geometries with structured meshes.

In applications involving cracks, the X-FEM is particularly effective. Such problems encompass discontinuities across crack surfaces and singularities, as well as steep gradients at crack fronts. In contrast, the classical FEM would require a mesh specially tailored to accommodate these features, which can be especially challenging when dealing with crack propagation in three dimensions. The X-FEM, on the other hand, can address these types of problems using fixed meshes and adapt to crack propagation through dynamic enrichment of the approximation.

The approach of simulating crack propagation using an enriched Finite Element Method was initially introduced by (Belytschko & Black, 1999), which encompassed three

key components: the description of the crack, the formulation of discretization, and the criteria for updating the crack. In this method, the task of mesh generation is simplified by enriching the elements located near the crack tip and along the crack faces. This enrichment is achieved by incorporating the leading singular crack tip asymptotic displacement fields using the Partition of Unity (PUM) method to account for the presence of the crack. In cases where multiple crack segments require enrichment using near-tip fields, a mapping algorithm is employed to align the discontinuity with the crack's geometry.

(Moës et al., 1999) introduced a more elegant and straightforward method for introducing a discontinuous field across the crack faces away from the crack tip. This was achieved by adapting the generalized Heaviside function and developing simple rules for the introduction of discontinuous and crack tip enrichments.

(Daux et al., 2000) introduced the concept of the junction function to account for multiple branched cracks and termed their approach the Extended Finite Element Method. They applied this method to model complex geometries, including multiple branched cracks, voids, and cracks emanating from holes, all without the need to mesh the geometric entities explicitly. The X-FEM offers promise because it eliminates the necessity for a mesh that conforms to cracks, voids, or inhomogeneities, as is typically the case with traditional FEM. In the X-FEM, an initial standard FE mesh for the problem is created without considering the geometric entity. The presence of cracks, voids, or inhomogeneities is independently represented, enriching the standard displacement approximation with additional functions. For crack modeling, both discontinuous displacement fields along the crack faces and the leading singular crack tip asymptotic displacement fields are incorporated into the displacement-based FE approximation using the PUM. Each enriched node's additional coefficients are independent.

(Stolarska et al., 2001) introduced an algorithm that combined the Level Set Method (LSM) with the X-FEM to model crack growth. The LSM was used to represent the crack location, including the positions of crack tips. (Moës et al., 2002) extended the X-FEM to handle arbitrary non-planar cracks in three dimensions. They described the crack geometry using two signed distance functions, which were capable of constructing a near-tip asymptotic field with a discontinuity conforming to the crack, even when it exhibited curvature or kinks near the tip.

(Ayhan & Nied, 2002) proposed an enriched Finite Element approach for calculating the Stress Intensity Factors (SIFs) in general three-dimensional crack problems. Sukumar and Prevost (2003) introduced the X-FEM for two-dimensional crack modeling in isotropic and bi-material media, integrated into the finite element program DynaflowTM. This approach was later employed by Huang, Sukumar, and Prévost (2003) for numerical modeling of SIFs in crack problems, including simulating crack growth.

(Stazi et al., 2003) presented a method for Linear Elastic Fracture Mechanics (LEFM) using enriched quadratic interpolations. In this method, the crack's geometry was represented by a level set function interpolated on the same quadratic finite element discretization. Lee et al. (2004) combined the X-FEM with the mesh superposition method (s-version FEM) for modeling both stationary and growing cracks. Their approach involved modeling the near-tip field using superimposed quarter-point elements on an overlaid mesh, with the rest of the discontinuity implicitly described by a step function on the Partition of Unity. The two displacement fields were matched through a transition region.

(Ventura et al., 2003) introduced a novel level set technique has been devised to represent surfaces that remain stationary while a moving front advances, such as cracks. The method combines very naturally with the extended finite element method (XFEM) where the discontinuous enrichment for cracks is best described in terms of level set functions. In this formulation, the level set is defined using a three-component tuple in two dimensions: the sign of the level set function and the coordinates of the closest point projection to the surface. The advancement of the level set is determined through geometric formulas, which can be easily put into practice. The results demonstrate the high accuracy of the method when applied to the growth of lines in two dimensions.¹⁹

(Budyn et al., 2004) introduced the X-FEM for simulating the growth of multiple cracks, even when they intersect, in both homogeneous and inhomogeneous brittle materials. This innovative method eliminates the need for remeshing as the cracks extend. Similarly, (Zi et al., 2004) presented a comparable approach for modeling the growth and merging of cracks within a quasi-brittle material containing multiple cracks.

Recent studies have delved into advanced aspects of Linear Elastic Fracture Mechanics (LEFM). In one such study, (Legrain et al., 2005) applied the X-FEM method to the realm

of large strain fracture mechanics, with a specific focus on analyzing the fracture of rubber-like materials.

(Moës et al., 2006) introduced a strategy aimed at imposing Dirichlet boundary conditions within the X-FEM framework. Their approach involved the construction of a corrected Lagrange multiplier space on the boundary, preserving the optimal rate of convergence.

(Ventura, 2006) presented a technique to eliminate the need for introducing quadrature sub-cells when employing discontinuous or non-differentiable enrichment functions in the X-FEM. This was achieved by replacing these functions with equivalent polynomials.

(Asadpoure et al., 2006) proposed an X-FEM methodology for modeling cracks in orthotropic materials. This approach relied on a discontinuous function and two-dimensional asymptotic crack tip displacement fields. In a subsequent work, (Asadpoure & Mohammadi, 2007) modified their previous model by introducing new enrichment functions to simulate orthotropic cracked media. The necessary near-tip enrichment functions were derived by extracting fundamental terms from complex solutions in the vicinity of the crack tip.

(Loehnert & Belytschko, 2007) harnessed the power of the X-FEM to explore the impact of crack shielding and amplification in various configurations of microcracks on the Stress Intensity Factors (SIFs) of a macro-crack. This study considered a large number of arbitrarily aligned microcracks.

(Sukumar et al., 2008) proposed a numerical technique for simulating non-planar three-dimensional elastic crack growth. They achieved this by combining the X-FEM with the fast marching method.

(Tabarraei et al., 2008) utilized the X-FEM on polygonal and quadtree finite element meshes to model two-dimensional crack growth. Their approach involved using the Laplace interpolant to construct basis functions on convex polygonal meshes, and the adoption of mean value coordinates for non-convex elements.

One of the primary challenges in the Extended Finite Element Method (X-FEM) is dealing with blending elements, which serve as connections between enriched and standard

elements. These elements are often crucial for ensuring the effective performance of local Partition of Unity (Melenk et al., 1996) enrichments. (Chessa et al., 2003) addressed this issue by employing the enhanced strain method within blending elements to enhance the performance of local PU enrichments. (Laborde et al., 2005) introduced a modification to the standard X-FEM approach to circumvent blending element problems in crack simulations. Their method involved enriching a fixed area around the crack tip.

(Legay et al., 2005) integrated the X-FEM into spectral finite elements for modeling gradients with discontinuities. In their approach, there was no need for blending elements when using high-order spectral elements. (Fries & Belytschko, 2006) developed an intrinsic X-FEM method that eliminated the need for blending elements when handling arbitrary discontinuities in the context of finite elements. This method avoided introducing additional unknowns at nodes intersected by discontinuities. (Fries, 2008) introduced a corrected X-FEM method that didn't encounter blending element issues. This approach was based on a weight function with a linearly decreasing profile for enrichment in the blending elements. (Gracie et al., 2008) presented a discontinuous Galerkin formulation that didn't rely on blending elements. Instead, they divided the domain into enriched and unenriched sub-domains and enforced continuity with an internal penalty method.

(Benvenuti et al., 2008) introduced a regularized X-FEM model for the transition from continuous to discontinuous displacements. In this model, strain and stress fields were modeled independently with specific constitutive assumptions.

(Belytschko et al., 2009) introduced a weight function blending method. They pre-multiplied the enrichment function with a smooth weight function, featuring compact support to enable a seamless transition between enriched and unenriched sub-domains.

(Tarancón et al., 2009) utilized higher-order hierarchical shape functions to mitigate unwanted effects of partial enrichment in blending elements. (Shibanuma et al., 2009) presented an alternative X-FEM formulation based on the PU FEM concept, which addressed the challenge of blending elements while ensuring numerical accuracy throughout the domain.

(Loehnert et al., 2011) extended Fries' corrected X-FEM method to three-dimensional cases, including finite deformation theory.

(Chahine et al., 2011) introduced a non-conformal approximation method known as the integral matching X-FEM. This method replaced the transition layer between the singular enrichment area and the rest of the domain with an interface associated with an integral matching condition of mortar type.

(Menk & Bordas, 2011) presented a technique to obtain stiffness matrices with condition numbers similar to those of standard FE matrices, without any enrichment, using a domain decomposition approach.

(Cheng et al., 2012) introduced a strain smoothing procedure within the X-FEM framework for Linear Elastic Fracture Mechanics (LEFM). This approach utilized edge-based smoothing to achieve a softening effect, resulting in stiffness matrices that were close to exact, leading to "super-convergence" and "ultra-accurate" solutions.

The utilization of static and quasi-crack analyses is a common practice in structural fracture analysis. However, these approaches serve as simplified models for highly complex dynamic phenomena and do not mirror real-world crack problems accurately. In the finite element method, dynamic problems are typically addressed by independently discretizing time and space. Time discretization is achieved through implicit or explicit time integration techniques, while spatial discretization is performed using standard finite element shape functions.

Dynamic crack analysis using XFEM encompasses some components. Firstly, a crack tracking procedure is necessary to represent an existing crack and its evolution over time. Unlike standard FEM, where a geometric representation of the crack is required (for example by aligning the mesh to the crack surfaces), in XFEM the functional representation of cracks (the crack location information resides inside the enrichment function, not the geometry) is obtained through the level set method and the fast marching approach. These have been successfully incorporated into XFEM codes and apply to both quasi-static and dynamic crack evolution problems.

The second component pertains to the formulation of dynamic crack propagation. (Belytschko et al., 2003) introduced a methodology that involves transitioning from a continuous to a discrete discontinuity when the governing partial differential equation loses hyperbolicity, particularly for rate-independent materials. This approach combines the

technique of hyperbolicity loss with XFEM cohesive crack models, allowing the computation of dynamic crack propagation direction and velocity by tracking the change in a hyperbolicity indicator. It has been employed to address problems involving crack branching. The concept of hyperbolicity loss was initially developed by (Gao et al., 1998) for the analysis of dynamic crack propagations, and subsequent studies by (Peerlings et al., 2002) and (Oliver et al., 2003) incorporated this technique into equilibrium equations.

Another major component involves the consideration of time integration schemes and the potential for a time-discontinuous XFEM. Subsequent refinements were introduced by m (Chessa & Belytschko, 2004) and (Chessa et al., 2006). They presented a locally enriched space-time extended finite element method for addressing hyperbolic problems with discontinuities. The coupling was achieved through a weak enforcement of flux continuity between the space-time and semi-discrete domains, akin to discontinuous Galerkin methods. The TXFEM was successfully applied to scenarios involving the Rankine-Hugoniot jump conditions for linear first-order wave and nonlinear Burgers equations.

Additionally, (Réthoré et al., 2005) introduced an energy-conserving scheme within the X-FEM framework for modeling dynamic fracture and time-dependent problems. Their approach demonstrated the stability of the numerical scheme in linear fracture mechanics. They proposed a combined space-time extended finite element method based on the principles of the time extended finite element method (TXFEM). This approach enabled the use of suitable time formulas that satisfied stability and energy conservation criteria. XFEM was used to implicitly define a virtual crack field tangential to the crack front, permitting the separation of mixed modes of fracture.

(Menouillard et al., 2006; Menouillard et al., 2008) presented an explicit time-stepping method that involved a mass matrix lumping technique for enriched elements. They showed that the critical time step for enriched elements is of a similar order as that for the corresponding non-enriched elements.

(Grégoire et al., 2007) conducted a dynamic crack propagation experiment aimed at replicating two significant phenomena: mixed-mode propagation and the intriguing behavior of crack stoppage and subsequent resumption. They elucidated this experiment through X-FEM simulations, utilizing a computational approach to analyze the underlying

mechanics. Their key insight lies in the application of a simplified fracture theory, which involves considering dynamic crack initiation toughness, aligning the crack's path with the maximum principal stress direction, and implementing a straightforward equation to calculate the crack's speed. This theory effectively captures and explains the experimental outcomes, shedding light on the observed complexities of crack propagation under different conditions.

(Nistor et al., 2008) presented a numerical implementation of XFEM for the analysis of crack propagation in structures subjected to dynamic loading. They introduce a new module, called DynaCrack, which is integrated into their dynamic FEM code, DynELA. This module is responsible for evaluating crack geometry, tracking crack propagation, and facilitating the post-processing of numerical results. It employs an explicit integration scheme to solve the system of discrete equations.

(Combescure et al., 2008) introduced an adaptive cohesive element formulation that addresses these challenges by adding new cohesive elements as the crack propagates, ensuring proper energy conservation during remeshing. They also highlight the effectiveness of the eXtended Finite Element Method (X-FEM) for simulating complex dynamic crack propagation and validate a two-dimensional version of this approach through experiments on a brittle isotropic plate.

(Elguedj et al., 2009) introduced a generalized mass lumping technique for explicit dynamics simulations using the X-FEM with arbitrary enrichment functions. This technique was based on an exact representation of the kinetic energy of rigid body modes and enrichment modes.

(Gravouil et al., 2009) presented a general explicit time integration technique for X-FEM dynamic simulations with a standard critical time step. They achieved this by developing an element-by-element strategy that coupled the standard central difference scheme with an unconditionally stable-explicit scheme.

(Fries & Zilian, 2009) investigated the convergence properties of different time integration methods within the X-FEM framework for moving interfaces. They studied one-step time-stepping schemes, the implicit Euler method, the trapezoidal rule, and the implicit midpoint rule.

(T. Menouillard & T. J. A. m. Belytschko, 2010) enriched the X-FEM using meshless approximation for dynamic fracture problems. This method employed mesh-free approximation to smooth the stress state near the crack tip during propagation, reducing unphysical oscillations in stress due to crack propagation.

(T. Menouillard & T. J. I. J. f. N. M. i. E. Belytschko, 2010) proposed a method based on enforcing the continuity of forces corresponding to enriched degrees of freedom to facilitate a smooth release of the tip element as the crack tip traverses through it.

(Menouillard et al., 2010) introduced a new enrichment method with a time-dependent enrichment function for dynamic crack propagation within the X-FEM framework. They studied the impact of different directional criteria on crack path predictions.

(D. Motamedi & S. J. E. F. M. Mohammadi, 2010; D. Motamedi & S. J. I. j. o. f. Mohammadi, 2010) conducted dynamic crack analyses for composites using orthotropic enrichment functions within the X-FEM framework. They evaluated dynamic SIFs using the domain separation integral method.

(Esna Ashari & Mohammadi, 2012) applied the X-FEM for fracture analysis of delamination problems in fiber-reinforced polymer reinforced beams. They modeled stress singularities near the debonding crack tip using orthotropic bimaterial enrichment functions.

(Liu et al., 2011) developed a higher-order X-FEM method based on the spectral element method for simulating dynamic fracture. This method effectively suppressed numerical oscillations and improved the accuracy of computed SIFs and crack path predictions.

(Motamedi & Mohammadi, 2012) introduced time-independent orthotropic enrichment functions for dynamic crack propagation of moving cracks in composites using the X-FEM. These enrichment functions were derived from analytical solutions for moving/propagating cracks in orthotropic media.

Another challenging part of dynamic fracture analysis concerns the determination of dynamic fracture properties. This includes defining fundamental concepts such as energy release rate, dynamic toughness, and stress intensity factors, as well as reformulating

contour integrals, equivalent domain integrals, and interaction integrals to account for the effects of velocity and acceleration terms. It also involves establishing the criteria for expressing dynamic crack propagation. For example, (Peerlings et al., 2002), (Belytschko et al., 2003) and (Oliver et al., 2003) adopted the original concept introduced by Gao and Klein (1998) and developed a methodology for transitioning from a continuum to a discrete discontinuity based on the loss of hyperbolicity, particularly in the case of rate-independent materials.

The significance of error estimation in numerical analysis with the Extended Finite Element Method (X-FEM) has been explored by several researchers. (Belytschko et al., 2003) conducted a convergence study for a variant of the X-FEM on cracked domains. They used a cut-off function to localize the singular enrichment area and demonstrated that the convergence error of their proposed variant follows an order of h for a linear Finite Element Method (FEM).

(Ródenas et al., 2008) presented a stress recovery procedure that offers accurate estimations of the discretization error in Linear Elastic Fracture Mechanics (LEFM) problems within the X-FEM framework. They applied the super-convergent patch recovery (SPR) technique to achieve this goal.

(Panetier et al., 2010) introduced a method for obtaining local error bounds in fracture mechanics contexts. They evaluated the discretization error for quantities of interest computed in the X-FEM using the concept of the constitutive relation error.

(Ródenas et al., 2010) introduced a recovery-type error estimator that provides upper bounds on the error in energy norm for LEFM problems using the X-FEM. This method ensures equilibrium at a local level.

(Shen et al., 2010; Shen & Lew, 2010) introduced an optimally convergent discontinuous Galerkin-based X-FEM for fracture mechanics problems. They achieved an optimal order of convergence compared to other variants of the X-FEM technique.

(Nicaise et al., 2011) performed an a priori error estimate on the standard X-FEM with a fixed enrichment area and the X-FEM with a cut-off function. They estimated the error on the Stress Intensity Factors (SIFs).

(Prange et al., 2012) presented a straightforward recovery-based error estimator for discretization error in X-FEM analyses of crack problems. They used enhanced smoothed stresses to enable error estimation for arbitrarily distributed cracks.

(Byfut & Schröder, 2012) introduced a higher-order X-FEM method by combining the standard X-FEM with a higher-order FEM method based on Lagrange-type and hierarchical tensor product shape functions. They demonstrated the methodological aspects necessary for hp-adaptivity in X-FEM to achieve exponential convergence.

(González-Albuixech et al., 2013) investigated the convergence rate of solutions obtained from the domain energy integral for computing SIFs in two-dimensional curved crack problems using the X-FEM.

(Rodenas et al., 2013) presented a technique for obtaining an accurate estimate of the error in energy norm using a moving least squares (MLS) recovery-based procedure for X-FEM problems.

(Rüter et al., 2013) proposed a goal-oriented a posteriori error estimator for X-FEM approximations in LEFM problems. This method enables the computation of upper bounds on the error of the J-integral, a key parameter in fracture mechanics.

Researchers have delved into more advanced concepts in the analysis of Elastic Linear Fracture Mechanics using the Extended Finite Element Method (X-FEM). (Park et al., 2009) developed a mapping method to integrate weak singularities resulting from enrichment functions in the Generalized Finite Element Method (G-FEM)/X-FEM. Their approach is applicable to two- and three-dimensional problems, including arbitrarily shaped triangles and tetrahedra.

(Mousavi et al., 2010) introduced an alternative Gaussian integration scheme to construct a Gauss quadrature rule over arbitrarily shaped elements in two dimensions without the need for partitioning. This method proved to be efficient and accurate for evaluating weak form integrals.

(Bordas et al., 2011; Bordas et al., 2010) investigated the accuracy and convergence of enriched finite element approximations by applying strain smoothing to higher-order

elements. They highlighted the benefits of strain smoothing in enriched approximations, especially when enrichment functions are polynomial.

(Mousavi et al., 2011a, 2011b) presented a higher-order X-FEM with harmonic enrichment functions for complex crack problems. They computed enrichment functions for the crack by solving the Laplace equation with specific boundary conditions.

(Legrain et al., 2011) used the X-FEM with quadtree/octree meshes, focusing on the enrichment of hanging nodes. They proposed an approach to enforce displacement continuity along hanging edges and faces.

(Richardson et al., 2011) developed a method for simulating quasi-static crack propagation by combining the X-FEM with a general algorithm for cutting triangulated domains. They introduced a simple and flexible quadrature rule based on the same geometric algorithm.

(Shibanuma et al., 2011) compared the reproductions of a priori knowledge in the original X-FEM and the PU-FEM-based X-FEM for crack analysis. They observed that the original X-FEM lacked accurate reproduction of a priori knowledge in the local enrichment area close to the crack tip, while the PU-FEM-based X-FEM accurately reproduced a priori knowledge over the entire enrichment.

(Fries & Baydoun, 2012) and (Baydoun & Fries, 2012) presented a method for two- and three-dimensional crack propagation that combined the advantages of explicit and implicit crack descriptions. They described a propagation criterion for three-dimensional fracture mechanics using the hybrid explicit–implicit approach.

(Minnebo, 2012) introduced a three-dimensional integral strategy for the numerical integration of singular functions in the computation of stiffness matrices and Stress Intensity Factors (SIFs) using the interaction integral method produced by the X-FEM in LEFM.

(Ventura, 2006) introduced an innovative approach that eliminates the need for subdivision of elements into quadrature sub-cells aligned with the discontinuity or introducing any additional approximation. It demonstrated how standard Gauss quadrature can be applied directly within the elements containing the discontinuity. This approach

maintains accuracy without the complexity of element subdivision, offering a robust solution for crack and material discontinuity problems.

(Ventura & Benvenuti, 2015) considered the replacement of the traditional discontinuous enrichment function with a continuous equivalent polynomial extending over the entire element domain. This modification allows for the utilization of standard Gaussian quadrature within elements intersected by the discontinuity.

(Benvenuti et al., 2012) proposed the Gauss quadrature of integrals of discontinuous and singular functions in the three-dimensional X-FEM analysis of regularized interfaces.

(González-Albuixech et al., 2013) introduced a curvilinear gradient correction based on level set information used for crack description within the X-FEM framework. This was applied to compute SIFs in curved and non-planar cracks.

(Amiri et al., 2014) presented a method based on local maximum entropy shape functions combined with enrichment functions used in Partition of Unity Methods (PUMs) to discretize problems in LEFM.

(Pathak et al., 2013) presented a simple and efficient X-FEM approach for modeling three-dimensional crack problems. They divided the crack front into piecewise curve segments and approximated the level set functions using higher-order shape functions.

(Agathos et al., 2018) introduced a 3D vector level set method, and enrichment strategy for XFEM, which involves the adoption of discontinuous linear enrichment functions as a replacement for the asymptotic near-tip functions. The level set values are obtained for advancing cracks through straightforward geometric operations, thus eliminating the necessity to solve differential evolution equations. They introduced two variants of the XFEM. The first variant achieves optimal convergence rates by using geometrical enrichment within a fixed volume around the crack front, avoiding conditioning issues. The second variant, employing linear enrichment, simplifies implementation and reduces computational overhead, but it offers convergence rates similar to standard finite elements.

For further in-depth exploration of the innovative and successful applications of the developed finite element method, it is recommended to refer to three dedicated books in this field, authored by (Mohammadi, 2008, 2012), and (Khoei, 2015).

In the forthcoming chapters, we embark on a detailed exploration of the application of the Extended Finite Element Method (XFEM) in the dynamic analysis of crack growth. Our comprehensive investigation encompasses a wide array of critical aspects, beginning with an exposition of the method's general principles. We delve into the intricacies of accounting for crack tip and surface enrichment, addressing the formation of stiffness, mass, and damping matrices, and the spatial and temporal integration of governing equations. Our journey also includes the balance recovery algorithm, the interaction integration method for calculating stress intensity factors, and the dynamic fracture criterion.

To validate the effectiveness of our methodology, we present a series of practical examples, offering empirical evidence of its utility. These examples encompass two static analyses, one focused on mode I and another exploring mixed mode conditions. We further scrutinize scenarios involving stationary cracks under mixed mode conditions, and transitions from stationary to mode I crack propagation. Finally, we show the efficiency of sub-parametric elements in the dynamic analysis of crack growth, particularly when dealing with irregular mesh configurations.

In the closing chapter, we consolidate our findings and present conclusions drawn from our research, summarizing the key insights obtained throughout this thesis. We also provide suggestions for future research endeavors and areas that warrant further investigation, ensuring that this study contributes to the ongoing advancement of knowledge and practice in the field of dynamic crack analysis.

2 Extended Finite Element Method

The XFEM workflow can be broken down into distinct stages, each contributing to its effectiveness and versatility. Initially, XFEM commences with the generation of a finite element mesh. This mesh is designed and constructed without specific consideration for any potential discontinuities that might exist within the material being analyzed. These discontinuities can take the form of cracks, voids, or any other localized changes in the material's properties. The core technique employed in XFEM to address these discontinuities is known as subdomain enrichment. It is worth mentioning that, as the crack evolves, the nodal DOFs are updated to reflect the changes in the displacement and rotation of nodes within the finite element mesh.

In the next step, XFEM introduces enriching functions that are derived from analytical solutions for the displacement field around the anticipated discontinuity. These enriching functions serve as a vital bridge between the discontinuity and the existing finite element mesh. They capture the behavior of the material near the discontinuity, allowing for more accurate simulations. To fully incorporate these enriching functions and their associated behavior, additional degrees of freedom are introduced at specific nodes within the finite element mesh. These nodes are strategically chosen to interact with the discontinuities. By doing so, XFEM effectively integrates the effects of the discontinuity into the model. This enrichment process enhances the model's ability to represent the localized changes in stress, strain, and other material behaviors around the discontinuity. It's important to note that while XFEM incorporates the effects of discontinuities into the model, it does so without providing an explicit representation of the discontinuity itself within the finite element network. Instead, XFEM relies on the mathematical constructs of enriching functions and additional degrees of freedom to capture and simulate the behavior near these discontinuities.

Introducing cracks in XFEM simulations involves specialized techniques like the Level Set Method. This method represents cracks using a "level set function", which is normally implemented by assigning values to mesh nodes in order to build a signed distance function to the crack. The zero-level set of this function defines the precise crack location. As the simulation progresses, the level set function evolves, accurately capturing the crack growth and its geometry. q

Another step is to choose crack propagation criterion, which are rules that determine when and how cracks in materials or structures should grow, like the maximum stress and maximum principal stress, focus on stress levels at the crack tip. Energy-based criteria, such as the strain energy release rate (G) and J-integral, consider the energy needed for crack extension. Fracture toughness criteria rely on a material's toughness properties. Mixed-mode criteria account for different loading modes. Damage accumulation criteria apply to cyclic loading and fatigue. Environmental factors can affect criteria in specific materials. Temperature and loading rate dependencies are considered as well. The choice of a criterion depends on the material and loading conditions, guiding decisions for design and maintenance.

In solving equilibrium equations akin to the Finite Element Method (FEM), analogous steps include forming stiffness and, if relevant, mass matrices for each finite element. These matrices quantify structural resistance to deformation and inertia in dynamic scenarios. Global assembly combines these matrices and external loads into a system of equations. Numerical techniques like direct solvers and iterative methods solve the system, yielding displacements and dynamic responses. Post-processing and visualization tools analyze and visualize results, crucial for understanding structural behavior.

Continuing in the subsequent section, we will provide a brief overview of the fundamentals of the extended finite element method, including crack modeling, matrix assembly, temporal and spatial integration schemes for the discontinuous governing equation, residual force nullification techniques, crack growth criteria, and other pertinent details.

2.1 General Principles of the Method

Let us consider a point, denoted as x , in the space R^2 (for two-dimensional problems) or R^3 (for three-dimensional problems), residing within the finite element model. Additionally, let N be the set of nodes, expressed as $N = \{n_1, n_2, \dots, n_m\}$, where m represents the number of nodes within an element. In this context, the function responsible for computing the enriched displacement approximation pertaining to that point can be defined as follows:

$$\mathbf{u}^h(x) = \sum_{\substack{I \\ n_I \in N}} \phi_I(x) \mathbf{u}_I + \sum_{\substack{J \\ n_J \in N^g}} \phi_J(x) \Psi(x) \mathbf{a}_J \quad (2-1)$$

In this expression, \mathbf{u}_I represents the degrees of freedom for displacement in conventional finite elements, \mathbf{a}_J denotes the additional degrees of freedom for displacement, related to the enrichment, $\phi_I(x)$ represents the shape function associated with node I in conventional finite elements, $\Psi(x)$ signifies the enrichment function, and N^g is a set of nodes defined as follows:

$$N^g = \{n_J: n_J \in N, \omega_J \cap \Omega_g \neq \emptyset\} \quad (2-2)$$

In Equation (2-2), ω_J represents the influence domain of the shape function $\phi_J(x)$ at node n_J , and Ω_g is the domain dependent on the geometry of the discontinuities, such as a crack surface or crack tip. In essence, N^g is a set of nodes that are in some way associated with the discontinuities. To clarify this concept, the influence domain for a node like J is illustrated in Figure 1. Essentially, for each node, the influence domain is a spatial region where the shape functions of that node have non-zero values. For nodes located on the edges of elements, their influence domains will encompass the neighboring elements connected to that node. In higher-order finite elements where nodes may exist within elements, the influence domain of such nodes will be limited to the element containing that node.

Furthermore, the determination of the enrichment function Ψ is dependent on the type of discontinuity and the available analytical conditions associated with it.

If we examine Equation (2-1), it becomes evident that on the right-hand side of the equation, the first part corresponds to the approximation used in conventional finite elements, which was already established. What holds paramount significance in this equation, and plays a fundamental role in the extended finite elements, is the second part of the expression. Indeed, it is within this segment that the discontinuities can be effectively modeled.

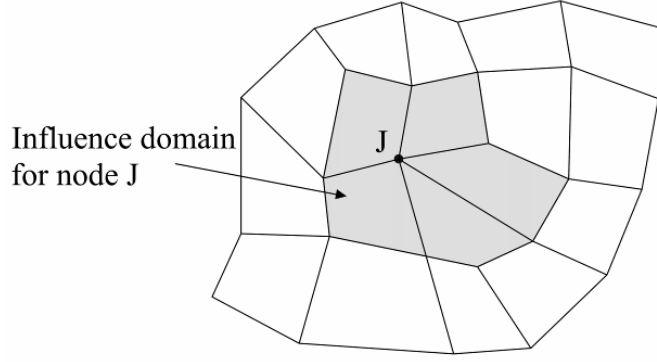


Figure 1- The influence domain for node J, when the node is positioned on the lateral face of the elements (Mohammadi, 2008).

2.2 Crack Modelling

In the extended finite element method, the modeling of cracks involves addressing two distinct aspects of the crack: the crack tips and the crack faces. The differentiation between these two aspects lies in the fact that around crack tips, there is a high concentration of stress, whereas in the case of crack faces, there is a discontinuity in displacement from the upper edge to the lower edge. Consequently, it becomes apparent that modeling these two aspects requires the use of two different types of enrichment functions. Equation (2-1) for modeling cracks within the entire domain is expressed as follows (Moës et al., 2002).

$$\mathbf{u}^h(x) = \sum_{n_I \in N} \phi_I(x) \mathbf{u}_I + \sum_{n_J \in N^R} \mathbf{b}_J \phi_J(x) H(x) + \sum_{k \in K^1} \phi_k(x) \left(\sum_I \mathbf{c}_k^I F_I(x) \right) \quad (2-3)$$

In which \mathbf{b}_J and \mathbf{c}_k^I represent additional degrees of freedom associated with nodes, $F_I(x)$ denotes two-dimensional displacement functions near the crack tips, and H (Daux et al.) is an Heaviside function.

2.2.1 Modeling Crack Surfaces and Heaviside Enrichment Function

As mentioned, for modeling crack faces, the function H is used. According to Figure 4, if e_n is the unit vector normal to the crack direction such that $e_s * e_n = e_z$ (where e_s is the

unit tangent vector), and the nearest point to x on the crack is denoted as x_I , then in this case:

$$H(x) = \begin{cases} +1 & ; (x - x_I) \cdot e_n > 0 \\ -1 & ; (x - x_I) \cdot e_n < 0 \end{cases} \quad (2-4)$$

In the case of no tip, the equation (2-3) turns into:

$$\mathbf{u}^h(x) = \sum_{n_I \in N} \phi_I(x) \mathbf{u}_I + \sum_{n_J \in N^R} \mathbf{b}_J \phi_J(x) H(x) \quad (2-5)$$

In Figure 2, a basic one-dimensional representation of the Heaviside function here as sign function) is displayed. Figure 3a demonstrates how the sign function emulates the presence of a discontinuity. So, the approximation (2-5) no longer functions as an interpolation method, and the field variable $\mathbf{u}(x)$ at an enriched node “I” does not equate to the nodal value \mathbf{u}_I .

$$\mathbf{u}^h(x) = \mathbf{u}_I + \mathbf{b}_J H(\xi_I) \neq \mathbf{u}_I \quad (2-6)$$

A simple shifting procedure guarantees the interpolation:

$$\mathbf{u}^h(x) = \sum_{n_I \in N} \phi_I(x) \mathbf{u}_I + \sum_{n_J \in N^R} \mathbf{b}_J \phi_J(x) (H(\xi) - H(\xi_J)) \quad (2-7)$$

In Figure 3b, you can observe the impact of the modified approximation on the one-dimensional crack problem. The enriched shape functions, when in their shifted form, become zero not only at node 2 but also at node 3. Consequently, the direct influence of enrichment is restricted solely to the central element that encompasses the discontinuity.

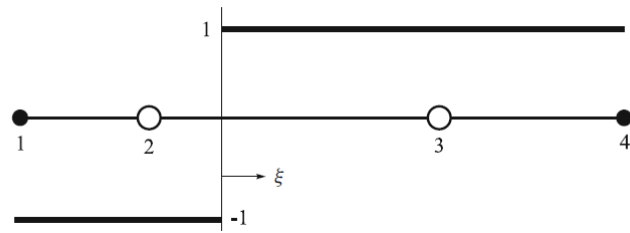
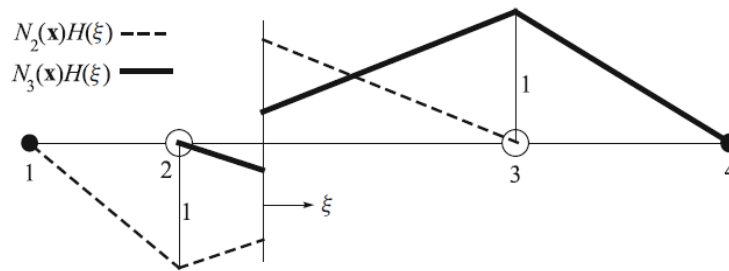
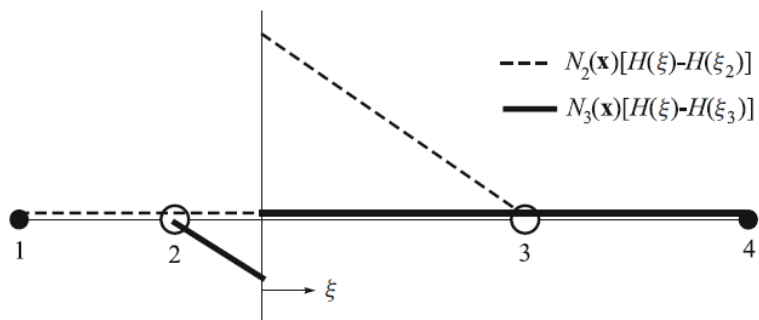


Figure 2-Heaviside function as $H(\xi)$



a) effect of sign function on shape functions



b) effect of shifting on shape functions

Figure 3-Enriched shape functions for nodes 2 and 3 and application of the shifting Heaviside function.

The overall jump in the displacement field can be obtained from:

$$\langle \mathbf{u}^h(x) \rangle = \mathbf{u}^h(x^+) - \mathbf{u}^h(x^-) = \dots = 2 \sum_{\substack{J \\ n_{J \in N^R}}} \mathbf{b}_J \phi_J(x) \quad (2-8)$$

The selection of nodes for Heaviside enrichment is performed in such a way that if there is a crack within the influence domain of a node without the crack tip being located in that domain, that node is enriched with the Heaviside enrichment function. These nodes enriched with the Heaviside function are indicated by circles in Figure 5.

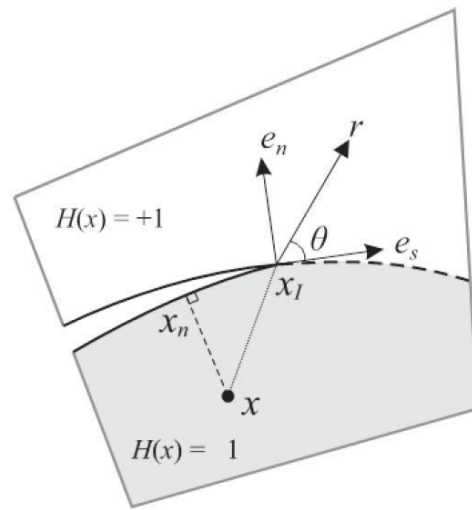


Figure 4- The local coordinates of the crack tip and the vectors that are normal and tangential to the extended Heaviside function at a point like x_I , which is the nearest point on the crack to the point x

In the selection of nodes for enrichment, choosing nodes for enrichment with the extended Heaviside function offers greater sensitivity because the incorrect selection of nodes can lead to solution instability. Let's assume that a crack has intersected several elements. If we denote the area of the elements related to a node that lies above the crack as A^+ and the area of the portion below the crack as A^- , and the total area of the elements as A , then the necessary condition for enriching that node with the extended Heaviside function is as follows:

$$\frac{A^+}{A} \geq mv \quad (2-9)$$

$$\frac{A^-}{A} \geq mv \tag{2-10}$$

In which mv represents the minimum allowable value, and in reference (Dolbow, 1999), it is suggested to consider a threshold value of 0.01% to circumvent numerical issues and solution instability. Figure 7 illustrates the determination of A^+ and A^- for node J.

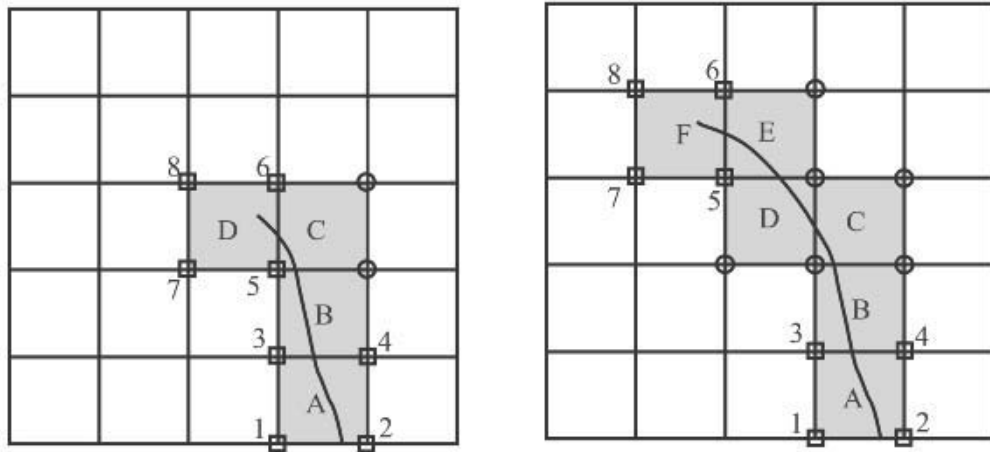


Figure 5- The selection of nodes for enrichment involves choosing nodes that are indicated by circles for enrichment with the extended Heaviside function and nodes that are indicated by squares for enrichment with functions near the crack tip (Mohammadi, 2008).

2.2.2 Modeling Crack Tip and Enrichment Functions

To simulate the complex deformation field near a crack tip accurately, it is necessary to employ functions that encompass all possible displacements within these equations. For a crack in a homogeneous isotropic body, functions can be chosen as follows (Dolbow et al., 2000).

$$\{F_1(r, \theta)\}_{l=1}^4 = \{\sqrt{r} \sin \frac{\theta}{2}, \sqrt{r} \cos \frac{\theta}{2}, \sqrt{r} \sin \theta \cos \frac{\theta}{2}, \sqrt{r} \sin \theta \sin \frac{\theta}{2}\} \quad (2-11)$$

In the above functions, (θ and r) are determined based on Figure 6 in the local coordinates centered at the crack tip. These functions represent the enrichment functions specific to crack tips, which should be utilized in the extended finite element elements within a homogeneous isotropic medium.

An important observation in Equation (2-11) is that the function $\sqrt{r} \sin \frac{\theta}{2}$ is not continuous. Specifically, it varies from $-\sqrt{r}$ to \sqrt{r} as θ ranges from $-\pi$ to π . This discontinuity characterizes the function along the two crack faces, whereas the other three functions converge to a common value on both sides of this interval. In other words, these three functions maintain the same value along the two crack faces. Figure 6 illustrates these functions.

Furthermore, the enrichment operation is only performed at nodes where the functions near the crack tip have an influence (as indicated by squares in Figure 5).

As a final point, to include the corrections related to interpolation failure of the enrichment, equation (2-3) can be rewritten as:

$$\begin{aligned} \mathbf{u}^h(x) = & \sum_{\substack{I \\ n_I \in N}} \phi_I(x) \mathbf{u}_I + \sum_{\substack{J \\ n_J \in NR}} \mathbf{b}_J \phi_J(x) (H(\xi(x)) - H(\xi(x_J))) \\ & + \sum_{k \in K^1} \phi_k(x) \left(\sum_I \mathbf{c}_k^l (F_l(x) - F_l(x_k)) \right) \end{aligned} \quad (2-12)$$

It's important to note that in the context of using the Heaviside function, only the elements intersected by the discontinuity are enriched. Specifically, when dealing with a crack tip, a region around the tip is also subject to enrichment. The concept of geometric enrichment, initially introduced by (Ventura et al., 2005) and further explored by (Laborde et al., 2005) in the same year, represents a significant advancement in the Extended Finite Element Method. Geometric enrichment enables a more precise representation of crack tips

by enhancing not only the elements intersected by the crack but also a region around the crack tip. This approach significantly improves the accuracy of XFEM simulations, particularly in the vicinity of crack tips or other singularities, without the need for excessive mesh refinement.

The size of the enrichment domain around the crack tip, often referred to as the "enrichment radius," stands as a crucial parameter in XFEM simulations. It determines the scope of the domain where the additional enrichment functions come into play. Selecting an appropriate enrichment radius is vital for achieving accurate results.

In our thesis, it is chosen to apply the enrichment techniques to only the elements that contain the crack surface and the immediate vicinity of the crack tip, using the appropriate enrichment functions.

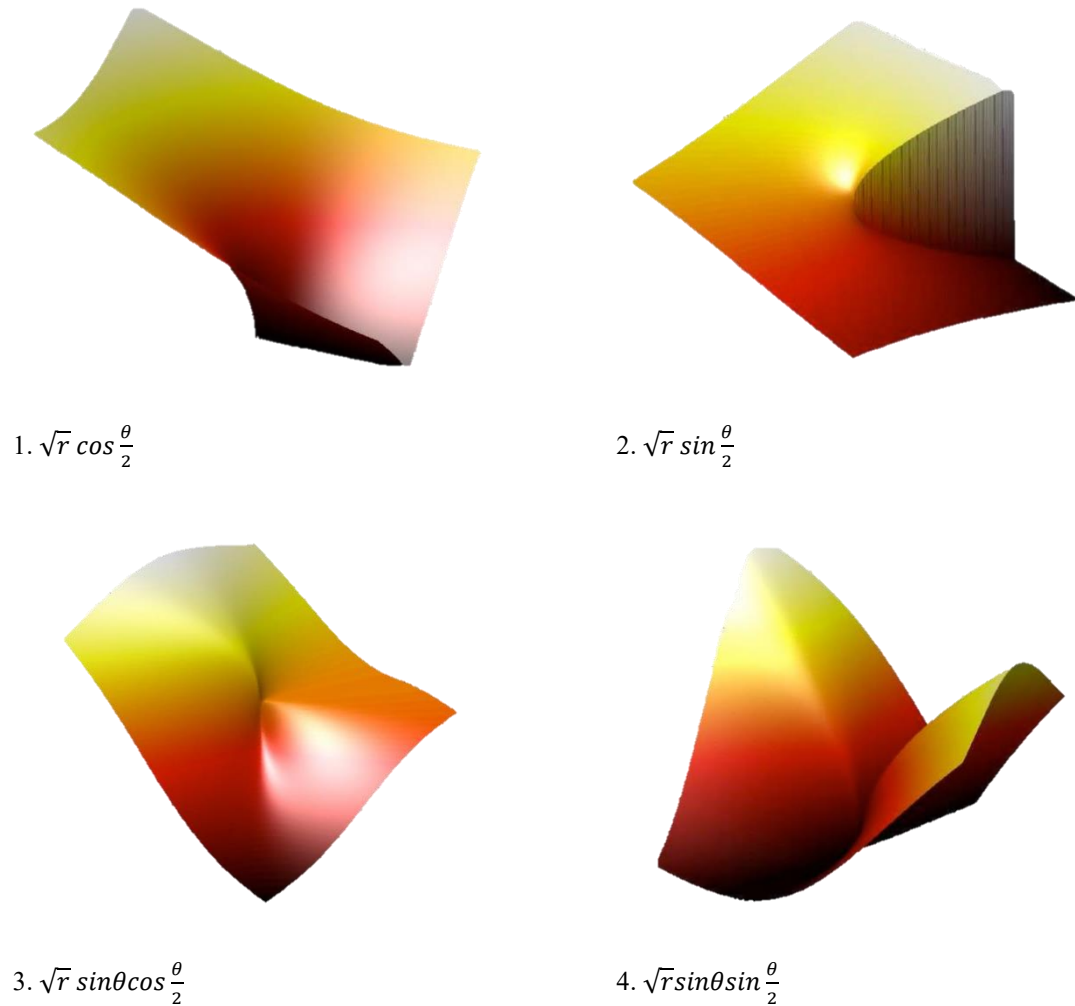


Figure 6 The enrichment functions near the crack tip, when the crack is positioned at the center of the parent element and the angle between the crack faces and the horizontal axis is $\pi/8$ (Mohammadi, 2008).

2.3 The implementation of the extended finite element method

Due to its primary advantages, the extended finite element method has found extensive applications in dynamic crack growth problems since its inception. (Chessa & Belytschko, 2004) introduced a method based on the elimination of hyperbolicity in dynamic equilibrium equation, transforming a continuous medium into a discontinuous one, and implemented it within the framework of the extended finite element method. (Belytschko & Chen, 2004; Chessa et al., 2006) then presented a spatiotemporal version of the extended

finite element method for dynamic problems with discontinuities. Other notable research includes the work by (Belytschko & Chen, 2004), where they proposed a singular element for dynamic crack growth problems. Additionally, there have been efforts to develop various formulations for the concentrated mass matrix in the extended finite element method, including studies by (Menouillard et al., 2006; Menouillard et al., 2008) and (Elguedj et al., 2009), with a focus on isotropic materials.

These research endeavors have significantly broadened the scope of the extended finite element method, making it a valuable tool for analyzing various dynamic crack growth problems in different material systems.

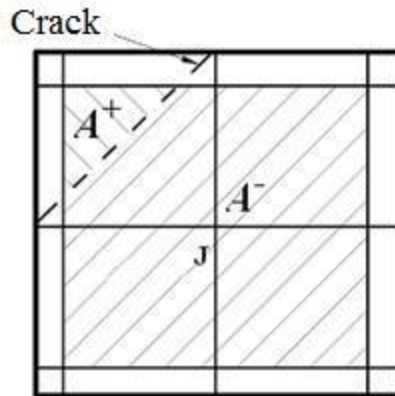


Figure 7- Determining A^+ and A^- for node J is discussed in reference(Mohammadi, 2012).

2.3.1 Formation of Matrices

The equations and matrices that need to be formed in the extended finite element method for solving problems follow a process very similar to the finite element method. The linearized, separated dynamic equations for the n -th time step in the extended finite element method are generally formulated as follows:

$$\mathbf{M}\ddot{\mathbf{u}}_n + \mathbf{C}\dot{\mathbf{u}}_n + \mathbf{K}\mathbf{u}_n = \mathbf{f}_n \quad (2-13)$$

In this context, where \mathbf{K} represents the stiffness matrix, \mathbf{M} represents the mass matrix, \mathbf{C} represents the damping matrix, \mathbf{u}_n denotes the displacement vector, $\dot{\mathbf{u}}_n$ represents the velocity vector, $\ddot{\mathbf{u}}_n$ represents the acceleration vector, and \mathbf{f}_n signifies the vector of external forces. The displacement vector encompasses both the finite element degrees of freedom and the additional degrees of freedom related to enrichments.

$$\mathbf{u}_n = \{d \ a \ b \}^T \quad (2-14)$$

Where “d” represents the degrees of freedom associated with finite elements, “a” represents the degrees of freedom related to surface discontinuities or cracks, and “b” represents the degrees of freedom associated with crack tips. The matrices that are generally derived should be obtained by computing and assembling the corresponding matrices for each element. The array “ij” of the mass and stiffness matrices, and the array “i” of the force matrix are calculated using the following relationships:

$$\mathbf{K}_{ij}^{rs} = \int_{\Omega^e} (\mathbf{B}_i^r)^T \mathbf{D} (\mathbf{B}_j^s) d\Omega \ ; \ (r, s = d, a, b) \quad (2-15)$$

$$\mathbf{M}_{ij}^{rs} = \int_{\Omega^e} \rho (\Phi_i^r) (\Phi_j^s) d\Omega \ ; \ (r, s = d, a, b) \quad (2-16)$$

$$\mathbf{f}_i^r = \int_{\partial\Omega \cap \partial\Omega} (\Phi_i^r) \bar{\mathbf{t}} d\Gamma + \int_{\Omega^e} (\Phi_i^r) \mathbf{b} d\Omega \ ; \ (r, s = d, a, b) \quad (2-17)$$

Where Ω^e represents the space of an element, Ω denotes the total problem domain, $\partial\Omega$ represents the boundaries of Ω , $\bar{\mathbf{t}}$ is the vector of applied forces on the boundaries, and \mathbf{b} is the vector of body forces. In equation (2-15), \mathbf{B} is the derivative matrix of shape functions, and Φ in equations (2-16) and (2-17) represents the shape functions, which consist of three parts corresponding to the finite element, and the enrichment using the Heaviside function, and the enrichments using crack tip functions.

The considered damping in this research is Rayleigh damping, which is related to the mass and stiffness matrices with two constant coefficients as follows:

$$\mathbf{C} = \gamma_k \mathbf{K} + \gamma_m \mathbf{M} \quad (2-18)$$

The values of γ_m and γ_k are established based on the preferred damping characteristics. The Rayleigh damping model offers the ability to regulate both proportional and non-proportional damping within a system.

- **Proportional Damping:** When γ_m equals zero, the damping is linked to the stiffness, and the damping ratio remains constant regardless of oscillation frequency. If γ_k is set to zero, the damping is exclusively related to the mass, and the damping ratio remains constant irrespective of oscillation frequency.

- **Non-Proportional Damping:** When both γ_m and γ_k are non-zero, damping combines both mass-proportional and stiffness-proportional elements, allowing the damping ratio to vary with oscillation frequency.

Typically, the values of γ_m and γ_k are chosen to align with the desired damping characteristics of the system. The Rayleigh damping model serves as a linear approximation of damping, and while it may not be suitable for all systems. It is important to note that Rayleigh damping coefficients are generally determined through the analysis of a system's response to known excitations or by means of experimental testing. The specific values can vary depending on the system in question and its intended dynamic behavior.

2.4 Methods of Spatial Integration

As previously mentioned, in the development of extended finite elements, it is necessary to employ functions for enrichment. Due to the discontinuous nature of some of these functions and their derivatives along the crack path, special considerations are required for integration. In cases like this, conventional Gauss's rule for integrating such discontinuous functions cannot yield precise results in the problem. In extended finite element method, to address this issue, element partitioning is usually employed. This means that if an element contains a crack and, as a result, one or more of its nodes are enriched with crack

tip functions or the Heaviside function, the element is divided into multiple subdomains for integration. The subdivision is typically done into sub-triangles and sub-quadrilaterals. A comprehensive explanation of this approach can be found for example in Dolbow's paper (Dolbow et al., 2001).

In the subdivision into sub-triangles method, elements intersecting with the crack, as shown in Figure 8, are divided into sub-triangles based on the crack's location. Each part on either side of the crack is subdivided into several triangles, and Gauss's rule is applied for integration within each of these triangles. This method is known for its suitable accuracy. For elements containing the crack tip, subdivision can be performed, considering the tip as one of the corners of the sub-triangles.

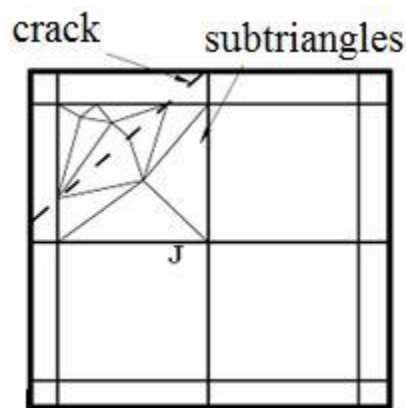


Figure 8- The subdivision of elements involved with cracks into sub-triangles for the purpose of integration (Mohammadi, 2012).

In the sub-triangles method, conditions (2-9) and (2-10) serve as both necessary and sufficient conditions for enrichment with the Heaviside function. This is because when a crack intersects one of the elements belonging to the domain of influence of a node, it inevitably leads to the creation of sub-triangles on both sides of the crack. Consequently, Gauss points will inevitably exist on both sides of the crack.

It is essential to emphasize that the subdivision is solely for the purpose of integration, and in practice, the element is not actually subdivided into multiple elements, nor are any additional degrees of freedom added to the problem.

2.5 Temporal Integration of the Dynamic Equilibrium Equation

Different methods are available for solving the system of equations (2-13), and in this research, two time integration methods are utilized: the Newmark time integration and the discontinuous Galerkin time integration. In problems where only dynamic external loading is applied, and cracks do not grow, the Newmark time integration method provides good results. To ensure unconditionally stable solutions, the Newmark method uses the coefficients α and β with values of 1/2 and 1/4, respectively.

The equations employed are as follows:

$$\begin{aligned}
 (\mathbf{M} + \beta\Delta t^2\mathbf{K} + a\Delta t\mathbf{C})\ddot{\mathbf{u}}_n \\
 = \mathbf{f}_n - \mathbf{K}\left(\mathbf{u}_{n-1} + \Delta t\dot{\mathbf{u}}_{n-1} + (1 - 2\beta)\frac{\Delta t^2}{2}\ddot{\mathbf{u}}_{n-1}\right) \\
 - \mathbf{C}(\dot{\mathbf{u}}_{n-1} - (1 - a)\Delta t\ddot{\mathbf{u}}_{n-1})
 \end{aligned} \tag{2-19}$$

$$\dot{\mathbf{u}}_n = \dot{\mathbf{u}}_{n+1} + (1 - a)\Delta t\ddot{\mathbf{u}}_{n-1} + a\Delta t\ddot{\mathbf{u}}_n \tag{2-20}$$

$$\mathbf{u}_n = \mathbf{u}_{n-1} + \Delta t\dot{\mathbf{u}}_{n-1} + (1 - 2\beta)\frac{\Delta t^2}{2}\ddot{\mathbf{u}}_{n-1} + \beta\Delta t^2\ddot{\mathbf{u}}_n \tag{2-21}$$

The Newmark method assumes the continuity of variables over time. Therefore, in problems where cracks grow, resulting in different stiffness matrices over consecutive time steps, the Newmark time integration can introduce numerical oscillations. These oscillations tend to grow over time and can even render the solution unstable in certain conditions.

To address this numerical issue, two highly effective methods exist in the technical literature: the discontinuous Galerkin method and the time extended finite element time method. Both methods share the same foundation and are based on the weighted residual method introduced by (Zienkiewicz & Dynamics, 1977). The essence of the Zienkiewicz method is to employ approximations of shape functions in time rather than using finite difference methods. The lowest degree of approximation that can be used for displacements

over time is the second degree (as the dynamic equilibrium equation is a second-order differential equation):

$$\mathbf{u}(t) = \sum_{i=n-1,n,n+1} N_i(t)\mathbf{u}_i \quad (2-22)$$

Where $N_i(t)$ represents the standard shape functions of a three-node bar element over time, and \mathbf{u}_i represents the displacement values at three time stations, namely $n-1$, n , and $n+1$. Instead of enforcing the strong form of the dynamic equilibrium equation at discrete points, the weighted residual form within an element of the extended finite element time integration method is satisfied in a weak sense over time, utilizing equation (2-25):

$$\int_{t_{n-1}}^{t_{n+1}} W(\mathbf{M} \sum \ddot{N}_i \mathbf{u}_i + \mathbf{C} \sum \dot{N}_i \mathbf{u}_i + \mathbf{K} \sum N_i \mathbf{u}_i - \sum N_i \mathbf{f}_i) dt = 0 \quad (2-23)$$

This equation is written specifically for a single time element and because the dynamic equilibrium equation is an ordinary differential equation with initial values, the displacement, velocity, and acceleration values at time steps n and $n-1$ are known. Therefore, in equation (2-23), there is only one unknown, u_{n+1} , which can be solved by selecting a weighting function, allowing the equation to be solved and progressing to the next time step. Zienkiewicz demonstrated that with different choices of weighting functions, various time integration methods (such as Newmark, central difference, Fox-Goodwin, etc.) can be obtained.

Now, the time extended finite element method, proposed by (Réthoré et al., 2005), is presented. Equation (2-22) is formulated based on the displacement approximation and establishes a relationship between the unknown displacement u_{n+1} and the known values from two time steps prior. Alternatively, velocity can be chosen as the primary unknown in which case the velocity approximation simply needs to be linear.

$$\mathbf{v} = \dot{\mathbf{u}} = \sum_{i=n,n+1} N_i \mathbf{v}_i \quad (2-24)$$

Where N_i are the standard shape functions of a two-node bar element.

$$N_n = \frac{t_{n+1} - t}{\Delta t}; N_{n+1} = \frac{t - t_n}{\Delta t} \quad (2-25)$$

Where $\Delta t = t_{n+1} - t_n$ and in this manner, the displacement is obtained from the integration of the velocity approximation (equation (2-27)).

$$\mathbf{u}(t) = \mathbf{u}_n + \int_{t_n}^t \mathbf{v}(\tau) d\tau = \frac{\mathbf{v}_{n+1}}{2\Delta t} (t - t_n)^2 + \frac{\mathbf{v}_n}{\Delta t} \left(t t_{n+1} - t_n t_{n+1} + \frac{t_n^2}{2} - \frac{t^2}{2} \right) \quad (2-26)$$

By substituting equation (2-24) for velocity and equation (2-26) for displacement into the following equation:

$$\int_{t_n}^{t_{n+1}} W(t) (\mathbf{M} \sum \dot{N}_i(t) \mathbf{v}_i + \mathbf{C} \sum N_i(t) \mathbf{v}_i + \mathbf{K} \mathbf{u}(t) - \sum N_i(t) \mathbf{f}_i) dt = 0 \quad (2-27)$$

The equation obtained is as follows (with the unknown \mathbf{v}_{n+1}).

$$\begin{aligned} (\mathbf{M} + \beta \Delta t^2 \mathbf{K}) \mathbf{v}_{n+1} \\ = -\Delta t \mathbf{K} \mathbf{u}_n + (\mathbf{M} + (\beta - \gamma) \Delta t^2 \mathbf{K}) \mathbf{v}_n + \Delta t ((1 - \gamma) \mathbf{f}_n \\ + \gamma \mathbf{f}_{n+1}) \end{aligned} \quad (2-28)$$

Where:

$$\frac{\beta}{2\Delta t} \int_{t_n}^{t_{n+1}} W(t) dt = \frac{1}{\Delta t^3} \int_{t_n}^{t_{n+1}} W(t)(t - t_n)^2 dt \quad (2-29)$$

$$\frac{\gamma}{\Delta t} \int_{t_n}^{t_{n+1}} W(t) dt = \frac{1}{\Delta t^2} \int_{t_n}^{t_{n+1}} W(t)(t - t_n) dt \quad (2-30)$$

Displacement is also obtained from equation (2-26):

$$\mathbf{u}_{n+1} = \mathbf{u}_n + \frac{\Delta t}{2} (\mathbf{v}_{n+1} + \mathbf{v}_n) \quad (2-31)$$

Acceleration at each time step is discontinuous and obtained from the following equation:

$$\mathbf{a}_{n+1} = \frac{(\mathbf{v}_{n+1} - \mathbf{v}_n)}{\Delta t} \quad (2-32)$$

It should be noted that equation (2-24) is still based on the continuity of velocity and is, therefore, not suitable for problems where crack propagation occurs. As suggested by (Réthoré et al., 2005), the Heaviside enrichment function should be added to the velocity approximation. If we consider the entire simulation time interval $[0, T]$ composed of Q time intervals with shape functions $\{N_i\}_{0,1,\dots,Q}$, then we have:

$$\mathbf{v}(t) = \sum_{i=0}^Q N_i \mathbf{v}_i^c + \sum_{j=0}^M \sum_{i \in Q_j} N_i H(t - t_j) \mathbf{v}_{i,j}^e \quad (2-33)$$

Where \mathbf{v}_i^c represents the standard degrees of freedom, $\mathbf{v}_{i,j}^e$ represents the additional degrees of freedom, and Q_j are the M time intervals enriched with the Heaviside function

$H(t - t_j)$. Since $H(t - t_j)$ is zero for all times $t_j > t$ and the influence range of the shape function N_j includes the interval $[t_{j-1}, t_{j+1}]$, $H(t - t_n)$ is only nonzero in the time interval $]t_n, t_{n+1}[$ (as shown in Figure 9).

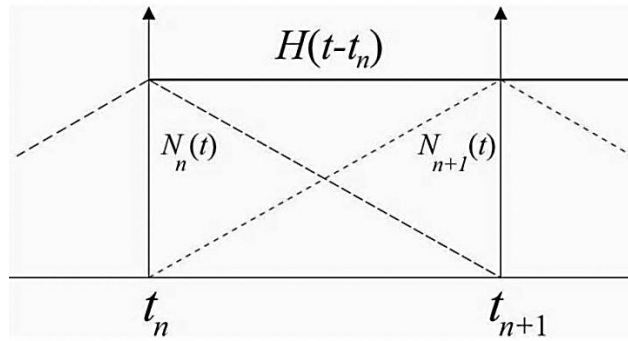


Figure 9- The Heaviside function's effect on the time-dependent shape functions

In the second term on the right-hand side of equation (2-33), used for approximating the non-polynomial part of the solution, discontinuities in velocity occur before and after each time station. Therefore, the velocity in each time interval $]t_n, t_{n+1}[$ is approximated as follows:

$$\mathbf{v}^c = \mathbf{v}_n^c N_n + \mathbf{v}_{n+1}^c N_{n+1} \quad (2-34)$$

$$\mathbf{v}^e = \mathbf{v}_{n+1}^e N_n H(t - t_n) \quad (2-35)$$

Where the additional degrees of freedom \mathbf{v}_{n+1}^e are equal to $\mathbf{v}_{n,n}^e$. The kinematic condition $\mathbf{u} - \dot{\mathbf{v}} = 0$ and the displacement continuity condition $u(t_n^+) - u(t_n^-) = 0$ are satisfied strongly through the following equations:

$$\mathbf{u}^c(t) = \mathbf{u}_n^c + \int_{t_n}^t \mathbf{v}^c(\tau) d\tau \quad (2-36)$$

$$\mathbf{u}^e(t) = \mathbf{u}_n^e + \int_{t_n^+}^t \mathbf{v}^e(\tau) d\tau \quad (2-37)$$

It's important to note that the velocity function is discontinuous at each time station, and therefore, its integration is discontinuous as well. Unlike the displacement continuity condition, the velocity continuity condition appears weakly in the weighted residual equation:

$$\begin{aligned} \int_{t_n^+}^{t_{n+1}^-} W(t) (\mathbf{M} \sum \dot{N}_i(t) \mathbf{v}_i \\ + \mathbf{C} \sum N_i(t) \mathbf{v}_i - \mathbf{K} \mathbf{u}(t) \\ - \sum N_i(t) \mathbf{f}_i) dt + W(t) \mathbf{M} (\mathbf{v}_n^+ - \mathbf{v}_n^-) = 0 \end{aligned} \quad (2-38)$$

Where

$$\mathbf{v}_n^+ = \mathbf{v}_n^c + \mathbf{v}_{n+1}^e \quad ; \quad \mathbf{v}_n^- = \mathbf{v}_n^c \quad (2-39)$$

Finally

$$\mathbf{v}_n^+ - \mathbf{v}_n^- = \mathbf{v}_{n+1}^e \quad (2-40)$$

Now, with the additional degrees of freedom and given values of \mathbf{v}_n^e , \mathbf{u}_n^e , \mathbf{v}_n^c , and \mathbf{u}_n^c , two unknowns \mathbf{v}_{n+1}^- and \mathbf{v}_{n+1}^e need to be solved for at the beginning and end of the time interval $]t_n, t_{n+1}[$. To achieve this, two weighting functions are required. If these two functions are taken as the same as the shape functions in equation (2-25), the following system of equations is obtained:

$$\begin{aligned}
& \begin{bmatrix} \mathbf{M} + \frac{\Delta t}{6} \mathbf{C} - \frac{\Delta t^2}{12} \mathbf{K} & -\frac{\Delta t}{6} \mathbf{C} - \frac{\Delta t^2}{12} \mathbf{K} \\ \frac{\Delta t}{2} \mathbf{C} + \frac{\Delta t^2}{3} \mathbf{K} & \mathbf{M} + \frac{\Delta t}{2} \mathbf{C} + \frac{\Delta t^2}{6} \mathbf{K} \end{bmatrix} \begin{bmatrix} \mathbf{v}_n^+ \\ \mathbf{v}_{n+1}^- \end{bmatrix} \\
& = \begin{bmatrix} \mathbf{F}_1 - \mathbf{F}_2 + \mathbf{M} \mathbf{v}_n^- \\ \mathbf{F}_1 + \mathbf{F}_2 + \mathbf{M} \mathbf{v}_n^- - \mathbf{K} \mathbf{u}_n^- \Delta t \end{bmatrix}
\end{aligned} \tag{2-41}$$

Where \mathbf{F}_1 and \mathbf{F}_2 are obtained based on the external loads in each time step as follows

$$\mathbf{F}_1 = \frac{\Delta t}{3} \mathbf{f}_n + \frac{\Delta t}{6} \mathbf{f}_{n+1}; \mathbf{F}_2 = \frac{\Delta t}{6} \mathbf{f}_n + \frac{\Delta t}{3} \mathbf{f}_{n+1} \tag{2-42}$$

The continuous displacement is also obtained from the integrals of equations (2-36) and (2-37):

$$\mathbf{u}_{n+1}^+ = \mathbf{u}_{n+1}^- = \mathbf{u}_n + \frac{\Delta t}{2} (\mathbf{v}_{n+1}^- + \mathbf{v}_n^+) \tag{2-43}$$

And for the acceleration:

$$\mathbf{a}_{n+1} = \left(\frac{\mathbf{v}_{n+1}^- - \mathbf{v}_n^+}{\Delta t} \right) \tag{2-44}$$

Using equations (2-41) to (2-43), continuous displacement is obtained at each time station, but velocity becomes discontinuous. As will be demonstrated in the numerical example, this formulation allows for stable modeling of dynamic crack growth.

The formulation presented in this section follows the approach of the time extended finite element method. The discontinuous Galerkin method, as proposed by (Li et al., 2003), is similar to this approach, with the difference that it uses a mixed formulation (velocity and displacement are separate quantities), and the constraint equation $\mathbf{u} - \dot{\mathbf{v}} = 0$ appears weakly in the weighted residual equation, unlike equations(2-36) and (2-37). The final equations of both methods are the same, and also in the discontinuous Galerkin

method, we arrive at the system of equations(2-41) and equations (2-42) to (2-44), after integration.

2.6 Balance Recovery During Crack Growth

When the crack grows and the element containing the crack tip changes, new degrees of freedom are added to the system, which initially have zero values (Figure 10). These zero values model the crack's geometric conditions in a wrong way. While the problem was in equilibrium at time step n , due to crack growth and changes in the stiffness matrix, mapping the values from time step n to the new configuration (time step $n+1$) can lead to the problem going out of equilibrium.

$$\mathbf{M}_n \ddot{\mathbf{u}}_n + \mathbf{C}_n \dot{\mathbf{u}}_n + \mathbf{K}_n \mathbf{u}_n = \mathbf{f}_n \quad (2-45)$$

But

$$\mathbf{M}_{n+1} \ddot{\mathbf{u}}_n^{n+1} + \mathbf{C}_{n+1} \dot{\mathbf{u}}_n^{n+1} + \mathbf{K}_{n+1} \mathbf{u}_n^{n+1} - \mathbf{f}_{n+1} = \mathbf{R} \neq 0 \quad (2-46)$$

In this context, X_n^{n+1} represents the mapping of degrees of freedom from the configuration at time step n to the configuration at time step $n+1$. The imbalance introduced in equation (2-46) before solving the system leads to numerical oscillations during the solution process, which can result in a deviation between the numerical solution and the actual physical response over time. To address this issue, (Réthoré et al., 2004) have suggested a procedure where the unbalanced system (equation (2-46)) is solved after the mapping step and before starting to solve the system of equations (equation (2-41)). By making a simplified assumption for velocity and displacement and then solving for acceleration:

$$\Delta \mathbf{u}_n^{n+1} + \Delta t^2 \beta \Delta \ddot{\mathbf{u}}_n^{n+1} \quad ; \quad \Delta \dot{\mathbf{u}}_n^{n+1} = \Delta t^2 \gamma \Delta \ddot{\mathbf{u}}_n^{n+1} \quad (2-47)$$

$$\mathbf{M}_{n+1}\Delta\ddot{\mathbf{u}}_n^{n+1} + \mathbf{C}_{n+1}\Delta\dot{\mathbf{u}}_n^{n+1} + \mathbf{K}_{n+1}\Delta\mathbf{u}_n^{n+1} - \mathbf{f}_{n+1} = -\mathbf{R} \quad (2-48)$$

Now it is possible to calculate the corrective values for acceleration, velocity, and displacement and then add these corrections to the original values. This approach is commonly used to correct numerical oscillations and maintain stability in dynamic simulations.

$$\ddot{\mathbf{u}}_n^{n+1} = \ddot{\mathbf{u}}_n^{n+1} + \Delta\ddot{\mathbf{u}}_n^{n+1}; \dot{\mathbf{u}}_n^{n+1} = \dot{\mathbf{u}}_n^{n+1} + \Delta\dot{\mathbf{u}}_n^{n+1}; \mathbf{u}_n^{n+1} = \mathbf{u}_n^{n+1} + \Delta\mathbf{u}_n^{n+1} \quad (2-49)$$

As will be illustrated in the numerical example, the execution of this procedure in conjunction with discontinuous time integration (equation (2-41)) will yield a notably robust stabilization in the resultant outcomes.

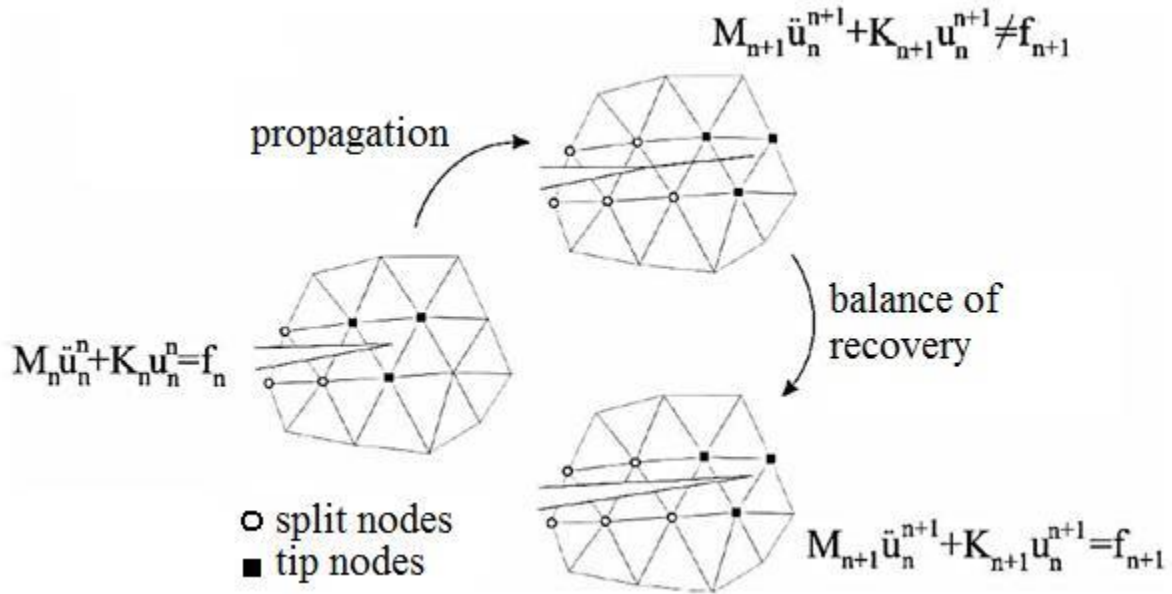


Figure 10- To maintain equilibrium during the mapping of degrees of freedom to the new configuration.

2.7 Calculating fracture parameters using the interaction integration (M_d)

In this thesis, mechanical fracture parameters are determined using the J-integral (M_d). The methodology employed here is adapted from the Nakamura formulation (Nakamura et al., 1995).

Firstly, it is essential to introduce the J-integral. One noteworthy feature of this approach is that, unlike methods that directly compute fracture parameters from the displacement fields near the crack tip through numerical solution (such as the displacement extrapolation method), the J-integral employs a finite domain around the crack tip and provides more accurate results, which are less sensitive to the numerical approximation near the crack tip. Furthermore, the J-integral maintains a constant value along any closed path around the crack tip, provided that no stress is imposed on the crack edges. This constant value, denoted as J_k^d for dynamic problems in the general coordinates $k=X, Y$, has been extended by (Nishioka & Atluri, 1980) as follows:

$$J_k^d = \int_{\Gamma+\Gamma_c} \left((w_s + w_d)n_k - t_i u_{i,k} \right) d\Gamma \quad (2-50)$$

$$+ \int_{A-A_1} \left((\rho \ddot{u}_i - f_i^b) u_{i,k} - \rho \dot{u}_{i,k} \dot{u}_{i,k} \right) dA$$

In which u_i , t_i , and f_i^b represent displacement, surface tractions, and body forces, and n_k is the normal vector component $n = (n_x, n_y)$. Additionally, Γ_1 , Γ , and Γ_c denote the paths of the near-field (obtained based on the assumption of small path, subsequently neglected), far-field, and crack surface. While A_1 and A represent the enclosed areas by these paths (see Figure 11). Furthermore, the strain energy density w_s and the kinetic energy density w_d are derived from the following relationships:

$$w_s = \frac{1}{2} \sigma_{ij} \varepsilon_{ij} \quad (2-51)$$

$$w_d = \frac{1}{2} \rho \dot{u}_i \dot{u}_i \quad (2-52)$$

Given that equation (2-50) necessitates integration along a path, numerical computations will be entirely dependent on the stress and displacement values at limited Gauss points. Any slight variation in the chosen path will result in the changing of points used in the integration. If errors occur at one or more limited points, these errors will manifest entirely in the final solution, and the selection of the path will be entirely dependent on the locations of the Gauss points.

To address such a problem, instead of integrating along a path, integration should be performed over a surface. To achieve this objective, (Kim et al., 2003) employed the divergence theorem and obtained the integral over a surface from equation (2-53), which, notably, exhibits better compatibility with the finite element method:

$$J_k^d = \int_A \left(\sigma_{ij} u_{i,k} - (w_s + w_d) \right) q_{,k} dA \quad (2-53)$$

$$+ \int_A \left((\rho \ddot{u}_i - f_i^b) u_{i,k} - \rho \dot{u}_{i,k} \dot{u}_{i,k} \right) q dA$$

Where the function q is selected in such a way that its value is set to zero at the nodes located on Γ or outside it, and it is set to one at the nodes inside Γ .

To numerically compute M_d in accordance with the finite element method, (Li et al., 1985) presented this integral over the integration surface as follows:

$$\begin{aligned}
 M_d = \int_A \left[\left(\boldsymbol{\sigma} \cdot \frac{\partial \mathbf{u}^{aux}}{\partial x_1} + \boldsymbol{\sigma}^{aux} \cdot \frac{\partial \mathbf{u}}{\partial x_1} \right) \frac{\partial q}{\partial x} - \left(\boldsymbol{\sigma} : \boldsymbol{\varepsilon}^{aux} + \rho \frac{\partial \mathbf{u}}{\partial t} \cdot \frac{\partial \mathbf{u}^{aux}}{\partial t} \right) \frac{\partial q}{\partial x_1} \right. \\
 + \left(\rho \frac{\partial^2 \mathbf{u}}{\partial t^2} \cdot \frac{\partial \boldsymbol{\sigma}^{aux}}{\partial x_1} + \frac{\partial \boldsymbol{\sigma}^{aux}}{\partial x} \cdot \frac{\partial \mathbf{u}}{\partial x_1} - \frac{\partial^2 u}{\partial t \partial x_1} \cdot \frac{\partial \mathbf{u}^{aux}}{\partial t} \right. \\
 \left. \left. - \frac{\partial \mathbf{u}}{\partial t} \cdot \frac{\partial^2 \mathbf{u}^{aux}}{\partial t \partial x_1} \right) q \right] dA
 \end{aligned} \tag{2-56}$$

The nodal values of the function q within the closed path Γ , as mentioned in the method, are depicted in Figure 12, where points with $q=1$ is represented in blue and $q=0$ in green. Therefore, the values of the q function at Gauss points inside elements where the nodal values of this function are not uniform can be determined using the nodal shape functions of those elements as follows:

$$q(x) = \sum_{i=1}^{nn} \varphi_i(x) q_i \tag{2-57}$$

Where “nn” is the number of nodes in the element containing point x , and $\varphi_i(x)$ represents the shape functions of that element.

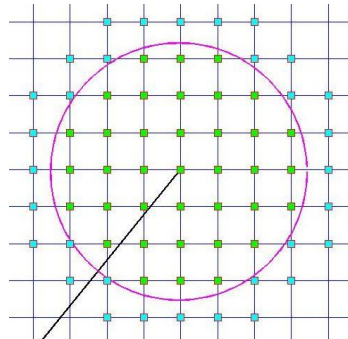


Figure 12- The nodal values of the q function in a regular finite element mesh, where $q=1$ is represented in blue and $q=0$ in green, are shown in the diagram.

Based on the calculated M_d , the dynamic stress intensity factors can be estimated using the following relationship:

$$M_d = \frac{2}{E'} [f_I(V_C)K_I K_I^{aux} + f_{II}(V_C)K_{II} K_{II}^{aux}] \quad (2-58)$$

By selecting an appropriate auxiliary field and setting $K_{II}^{aux} = 0$ and $K_I^{aux} = 1$, as well as $K_{II}^{aux} = 1$ and $K_I^{aux} = 0$, one can compute K_I and K_{II} . The functions $f_I(V_C)$ and $f_{II}(V_C)$ are obtained from the following relationships:

$$f_I(V_C) = \frac{4\beta_d(1 - \beta_s^2)}{(k + 1)D(V_C)} \quad ; \quad f_{II}(V_C) = \frac{4\beta_s(1 - \beta_s^2)}{(k + 1)D(V_C)} \quad (2-59)$$

Where for the plane strain condition, $k = 3 - 4\nu$ and for the plane stress condition, $k = \frac{3-\nu}{1+\nu}$, and the remaining parameters are defined as follows:

$$\beta_d^2 = 1 - \frac{V_C^2}{C_d^2} \quad ; \quad \beta_s^2 = 1 - \frac{V_C^2}{C_s^2} \quad (2-60)$$

$$D(V_C) = 4\beta_d\beta_s - (1 + \beta_s^2)^2 \quad (2-61)$$

The expansion waves' speeds, C_d , and shear waves' speeds, C_s , are obtained using Lamé coefficients. Additionally, the Rayleigh wave speed, C_R , in various references (Malischewsky, 2005; Rahman & Michelitsch, 2006; Vinh & Malischewsky, 2006; Vinh & Malischewsky, 2008; Vinh & Malischewsky, 2007) is expressed through different formulas as a function of the Poisson's ratio.

$$C_d = \sqrt{\frac{\lambda + 2\mu}{\rho}} \quad ; \quad C_s = \sqrt{\frac{\mu}{\rho}} \quad (2-62)$$

2.8 Dynamic Fracture Criterion

In dynamic crack modeling, it is essential to have a criterion for describing the stability of an existing crack. After determining the instability of the crack, a criterion is also needed to determine the growth angle and rate. The fundamental idea for assessing the stability or instability of a crack involves comparing the stress intensity factor with the critical dynamic stress intensity factor, which depends on material properties and requires experimental methods for its determination. If the crack becomes unstable under this criterion and starts to propagate, the growth angle can be determined using criteria such as the maximum hoop stress.

During crack growth, the growth rate will reach a value where the maximum hoop stress intensity factor becomes equal to the dynamic growth rate. To estimate the dynamic growth rate, (Kanninen et al., 1988) proposed to use the pseudo-static fracture toughness instead of the dynamic fracture toughness. In this approach, the dynamic growth rate is considered as follows (Grégoire et al., 2007):

$$\left\{ \begin{array}{ll} K_{tt} < K_{Ic}^d & \text{stable crack} \\ K_{tt}(t, 0) = K_{Ic}^d & \text{crack initiation at } \theta = \theta_c \\ K_{tt}(t, V_c) \geq K_{Ic}^d \Rightarrow K_{tt}(t, V_c) = K_{Ic}^D(V_c) & \text{crack propagation} \end{array} \right. \quad (2-63)$$

Where K_{tt} represents the maximum hoop dynamic stress intensity factor, K_{Ic}^d is the initial dynamic fracture toughness, and K_{Ic}^D is the crack growth toughness, as defined in the references (Elguedj et al., 2009; Grégoire et al., 2007).

$$K_{Ic}^D = \frac{K_{Ic}^d}{\left(1 - \frac{V_c}{C_R}\right)} \quad (2-64)$$

Where V_c can be calculated as follows, based on the references (Freund et al., 1982; Freund, 1998):

$$V_c = C_R \left(1 - \frac{K_{Ic}^d}{K_{tt}} \right) \quad (2-65)$$

However, (Menouillard et al., 2010) used the following relationship:

$$V_c = C_R \left(1 - \left(\frac{K_{Ic}^d}{K_{tt}} \right)^2 \right) \quad (2-66)$$

2.9 Sub-parametric element

In finite element analysis, shape functions are mathematical functions that are used to discretize geometry and displacement over the elements. These shape functions are typically chosen based on the order or degree of polynomial interpolation.

In iso-parametric elements, the same interpolation functions, or shape functions, are used for both the geometry (mapping from a reference element) and the field variables. However, in a sub-parametric approach, lower-order shape functions are employed, which means that the degree of polynomial interpolation is reduced.

The sensitivity to element distortion is a critical consideration when choosing the type of finite element for an analysis. It's important to understand that not all finite elements respond to distortion in the same way. Iso-parametric elements employ higher-order shape functions (in comparison with sub-parametric elements), which are designed to provide more accurate approximations of both the geometry and the field variables. However, the drawback is that these higher-order shape functions can become unstable and even break down when an element experiences significant distortion. This sensitivity to distortion can result in convergence problems and inaccurate results, particularly in cases where the deformation is substantial, or the mesh quality is poor. In contrast, sub-parametric elements use lower-order shape functions. While these shape functions may not capture highly complex geometries with the same level of accuracy as Iso-parametric elements, they

exhibit greater robustness and stability when elements become distorted. They can handle such distortions without encountering the same level of numerical instability.

The Jacobian matrix represents the derivative of the mapping function that relates the coordinates in the reference element to those in real, physical space. It allows to account for the distortions that occur when mapping the element from a simple reference shape to the actual shape in the physical domain. This transformation is essential for computing integrals, gradients, and other mathematical operations in FEM.

When the mesh is irregular, and the Jacobian matrix varies significantly within an element in finite element analysis, it leads to some errors in various aspects of the analysis. Integration errors occur due to inaccurate transformations from the physical to the reference domain, affecting computed quantities like stress and strain. Stiffness matrix errors arise because the relationship between nodal displacements and forces relies on accurate derivatives of shape functions and the Jacobian matrix. Convergence issues arise in iterative solvers due to Jacobian variations within elements, causing slow or failed convergence, especially in nonlinear or transient analyses. Highly distorted elements lead to ill-conditioned stiffness matrices, making it challenging to solve equations and causing numerical instability. Using triangular elements with three nodes (3-node elements) can indeed be a way to mitigate the issue of varying Jacobian matrices within an element when the mesh is irregular. In a triangular element, as long as the nodes are not collinear, the Jacobian matrix will have a constant value within the element. This feature makes triangular elements a popular choice for modeling irregular or distorted geometries because they are less sensitive to mesh distortions compared to quadrilateral elements.

As previously mentioned, the quadrilateral shape function is employed for discretizing the field variables. However, when it comes to discretizing the geometry, a method involving the subdivision of each quadrilateral element into two sub-triangles is employed. Subsequently, Gaussian quadrature rules are applied within each of these triangles. It is worth noting that each triangle is defined in the s-t domain, with this domain being defined on the interval $[0,1]$.

In the context of FEM framework, the B matrix represents the matrix comprising the derivatives of the shape functions, dN/dx and dN/dy . These derivatives are determined through the mapping process from the reference element (ξ, η) to the physical element

(x,y), and the associated Jacobian matrix, as defined by equation (2-67) and (2-68). Furthermore, it is pertinent to note that at each Gaussian integration point, the derivatives $dN/d\xi$, $dN/d\eta$ and are calculated using the 4-node shape functions.

$$\begin{bmatrix} dN/dx \\ dN/dy \end{bmatrix} = \begin{bmatrix} d\xi/dx & d\eta/dx \\ d\xi/dy & d\eta/dy \end{bmatrix} \begin{bmatrix} dN/d\xi \\ dN/d\eta \end{bmatrix} \quad (2-67)$$

$$(2-68)$$

$$\begin{bmatrix} dN/d\xi \\ dN/d\eta \end{bmatrix} = J \begin{bmatrix} dN/dx \\ dN/dy \end{bmatrix}; \quad J^{-1} = \begin{bmatrix} d\xi/dx & d\eta/dx \\ d\xi/dy & d\eta/dy \end{bmatrix}$$

Indeed, given the discretization of geometry within the s-t domain, an initial step involves mapping the Gaussian points to the interval [-1,1]. This mapping process results in the decomposition of the Jacobian matrix into two distinct matrices, namely J_1 and J_2 .

$$J = \begin{bmatrix} dx/d\xi & dy/d\xi \\ dx/d\eta & dy/d\eta \end{bmatrix} = \begin{bmatrix} ds/d\xi & dt/d\xi \\ ds/d\eta & dt/d\eta \end{bmatrix} \begin{bmatrix} dx/ds & dy/ds \\ dx/dt & dy/dt \end{bmatrix} \quad (2-69)$$

$$J = J_1 * J_2 \quad (2-70)$$

To calculate J_1 , one can simply apply the definition of discretization using shape functions. Here, ξ_i and η_i represent the coordinates of the corners of the triangle within the [-1,1] domain, while $N_i^{tri}(s,t)$ signifies the Lagrangian triangular shape functions.

$$J_1 = \begin{bmatrix} ds/d\xi & dt/d\xi \\ ds/d\eta & dt/d\eta \end{bmatrix} \quad (2-71)$$

$$\begin{cases} \xi = \sum \xi_i * N_i^{tri}(s,t) \\ \eta = \sum \eta_i * N_i^{tri}(s,t) \end{cases} \quad (2-72)$$

Following this, we obtain:

$$A = \begin{bmatrix} d\xi/ds & d\eta/ds \\ d\xi/dt & d\eta/dt \end{bmatrix} = \begin{bmatrix} \sum \xi_i * dN_i^{tri}/ds & \sum \eta_i * N_i^{tri}/ds \\ \sum \xi_i * dN_i^{tri}/dt & \sum \eta_i * N_i^{tri}/dt \end{bmatrix} \quad (2-73)$$

$$J_1 = inv(A) \tag{2-74}$$

To compute J_2 , we apply the definition of discretization using triangular shape functions ($N_i^{tri}(s, t)$). In this context, x_i and y_i represent the coordinates of the corners of the triangles in the physical element.

$$\begin{cases} x = \sum x_i * N_i^{tri}(s, t) \\ y = \sum y_i * N_i^{tri}(s, t) \end{cases} \tag{2-75}$$

$$J_2 = \begin{bmatrix} dx/ds & dy/ds \\ dx/dt & dy/dt \end{bmatrix} = \begin{bmatrix} \sum x_i * dN_i^{tri}/ds & \sum y_i * N_i^{tri}/ds \\ \sum x_i * dN_i^{tri}/dt & \sum y_i * N_i^{tri}/dt \end{bmatrix} \tag{2-76}$$

3 Examples

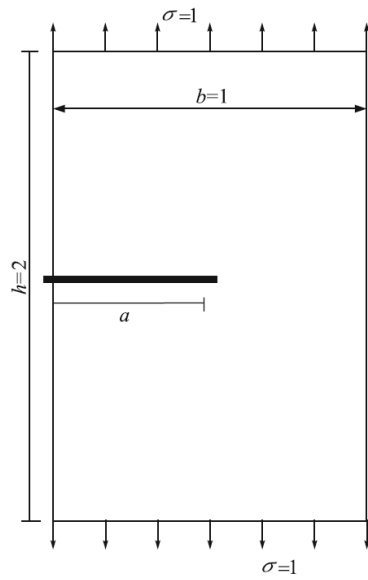
This section is dedicated to the validation of various components within the proposed framework, achieved through the simulation of several examples of fracture mechanics using X-FEM. To facilitate result comparison, stress intensity factors are computed utilizing the interaction integral method. These examples encompass two static analyses, one in mode I and another in mixed mode. Furthermore, we explore scenarios involving a stationary crack under mixed mode conditions and another case in which a crack is initially stationary and subsequently transitions to a moving mode I crack. Lastly, we engage in a discussion concerning different methods employed in dynamic analyses, and finally emphasis on showcasing the efficiency of sub-parametric elements in the dynamic analysis of crack growth, particularly in the presence of irregular mesh configurations. Note that in our thesis, only the elements that contain the crack surface and the one which contains the crack tip are enriched.

3.1 An Edge Crack in a Finite Plate

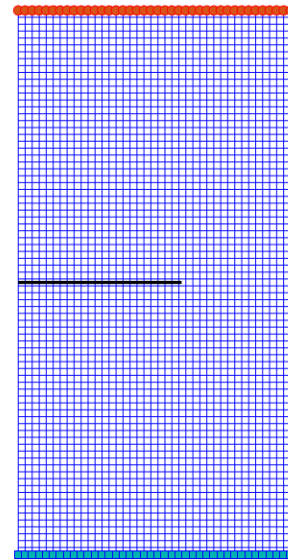
The first instance involves a finite plate under tensile stress containing a crack along its edge, as illustrated in Figure 13. To model this scenario, uniform finite element grids are employed, varying the length of the crack. Table 1 presents a comparison of the normalized mode I stress intensity factor, which is calculated as $K_I/\sigma\sqrt{\pi a}$, across different meshes and varying crack lengths 'a'. The numerical findings closely align with the analytical solution, demonstrating a strong agreement.

Table 1-Evaluating XFEM predictions for stress intensity factor against the analytical solution across various crack sizes.

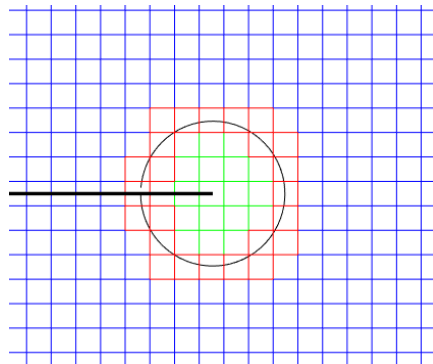
a/b	Analytical	XFEM	
		20*40	40*80
0.3	1.612	1.6103	1.5921
0.45	2.877	2.8854	2.8439
0.6	5.29	5.3271	5.3365



(a)



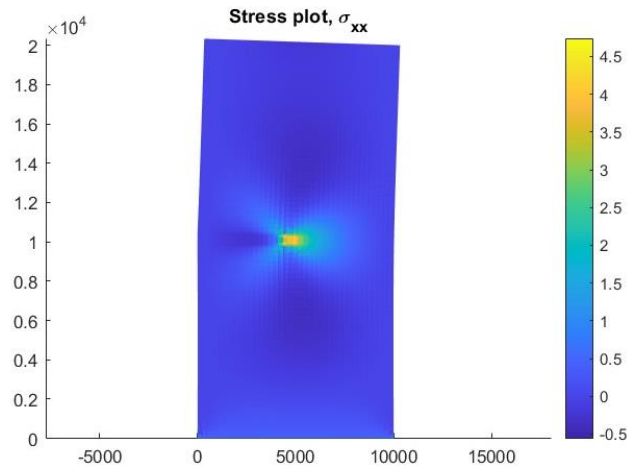
(b)



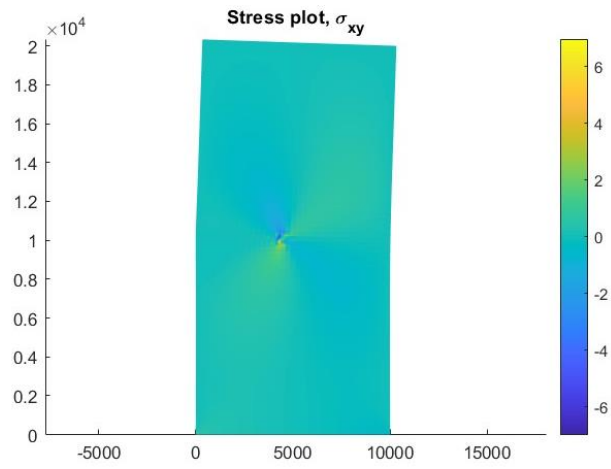
(c)

Figure 13-Geometry of the tensile plate with an edge crack(a), the finite element mesh, and the M-integral domain.

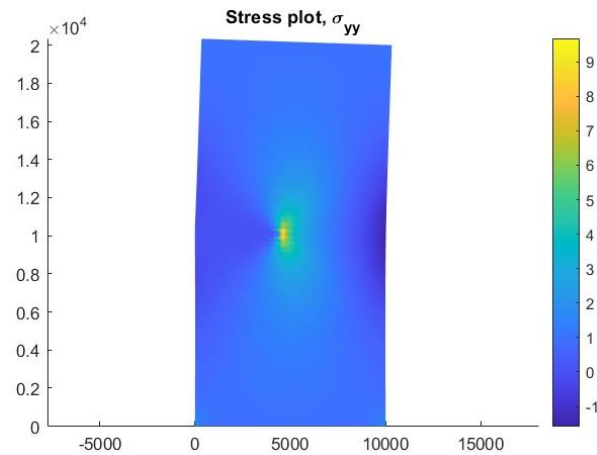
Figure 14 displays the distribution of stress components σ_{xx} , σ_{yy} and σ_{yx} on the deformed shape of the plate. It is evident from the illustration that XFEM effectively captures the singular nature of the stress field.



(a)



(b)



(c)

Figure 14- stress contours on the deformed shape of the plate a) σ_{xx} , b) σ_{yy} , c) σ_{xy} .

3.2 Tensile Plate with a Central Inclined Crack

This example is focused on a classical mixed-mode fracture problem, involving a tensile plate with a centrally inclined crack. The simulation employs a uniform structured finite element mesh, as illustrated in Figure 15. Stress intensity factors for all crack angles are computed using this fixed mesh. Table 2 presents a comparison between the normalized stress intensity factors predicted by XFEM for different crack angles and the analytical solution. Remarkably, there is a high degree of agreement between the XFEM predictions and the analytical results for all crack angles.

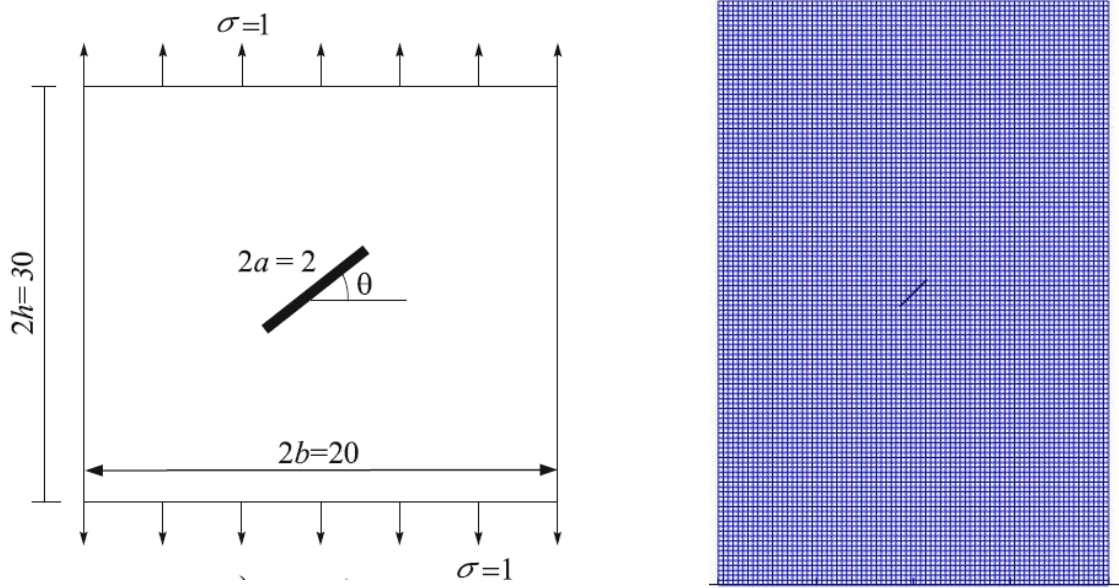


Figure 15- Geometry and the mesh for the mixed mode central crack problem.

3.3 Stationary mixed mode crack

In this instance, we examine the issue previously explored by Lee and Freund in 1990. Their analysis involved a semi-infinite plate containing a notched edge and subjected to an initial impact velocity, denoted as V_0 . The problem is characterized by mixed-mode behavior due to the absence of traction on the crack surfaces. Notably, the stress intensity factor for Mode I becomes negative when the lower part of the specimen makes contact with the upper part. The focus is to compute two dynamic stress intensity factors, KI and

KII. Figure 16 provides an overview of the geometry and the applied load. The specific dimensions involved are as follows: $H = 6$ meters, $a = 1$ meter, and $L = 4$ meters. The prescribed velocity at the boundary is $V_0 = 16.5$ meters per second. Two different meshes have been employed, one consisting of 40×60 four-node elements and the other of 60×120 . The material behavior is characterized as linear elastic, and the material properties are detailed in Table 3. For this problem, an analytical solution exists for both stress intensity factors as a function of time, as documented in (Lee & Freund, 1990) and (Ravi-Chandar, 2004).

Table 2-Evaluating the normalized mode I and II stress intensity factors against the analytical solution across various crack angles.

Theta	$K_I/\sigma\sqrt{\pi a}$		$K_{II}/\sigma\sqrt{\pi a}$	
	Analytical	XFEM	Analytical	XFEM
0.00	1.00	1.049000752	0.00	0.001395185
15.00	0.93	0.979708939	0.25	0.267352783
30.00	0.75	0.705333844	0.43	0.397501069
45.00	0.50	0.47278397	0.50	0.497026649
60.00	0.25	0.206426728	0.43	0.38449302
75.00	0.07	0.063794926	0.25	0.264819327

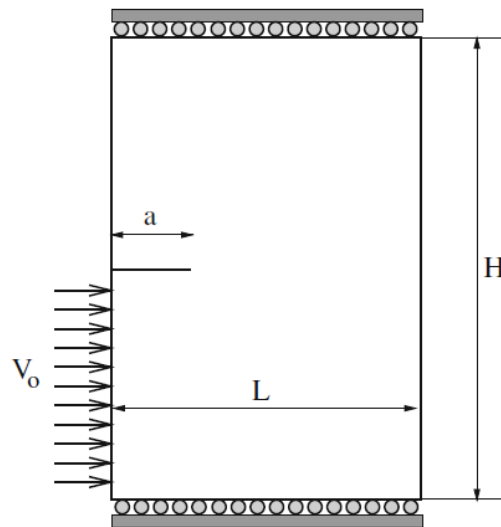


Figure 16-Geometry and Loading

Since the analytical solution applies to an infinite plate, its validity for a finite plate is limited until the reflected wave reaches the crack tip after being reflected from the right edge of the structure. The time taken for the wave to initially reach the crack tip is represented as t_c and is calculated as a/C_d , where C_d represents the dilatational wave speed. Subsequently, the computational analysis is conducted until $3 * t_c$. The stress intensity factors are normalized using a specific formula, which involves material properties and boundary conditions, as $-EV_0\sqrt{a/\pi}/(2C_d(1 - v^2))$. It's worth noting that an analytical solution is available for both stress intensity factors over time, as documented by (Lee & Freund, 1990).

Table 3- Material properties

Young's modulus (GPa)	Poisson's ratio	Density(kg/m ³)
200	0.25	7833

Figure 17 graphically displays the two normalized stress intensity factors, KI and KII, as functions of time. These results are obtained for different mesh sizes as mentioned before.

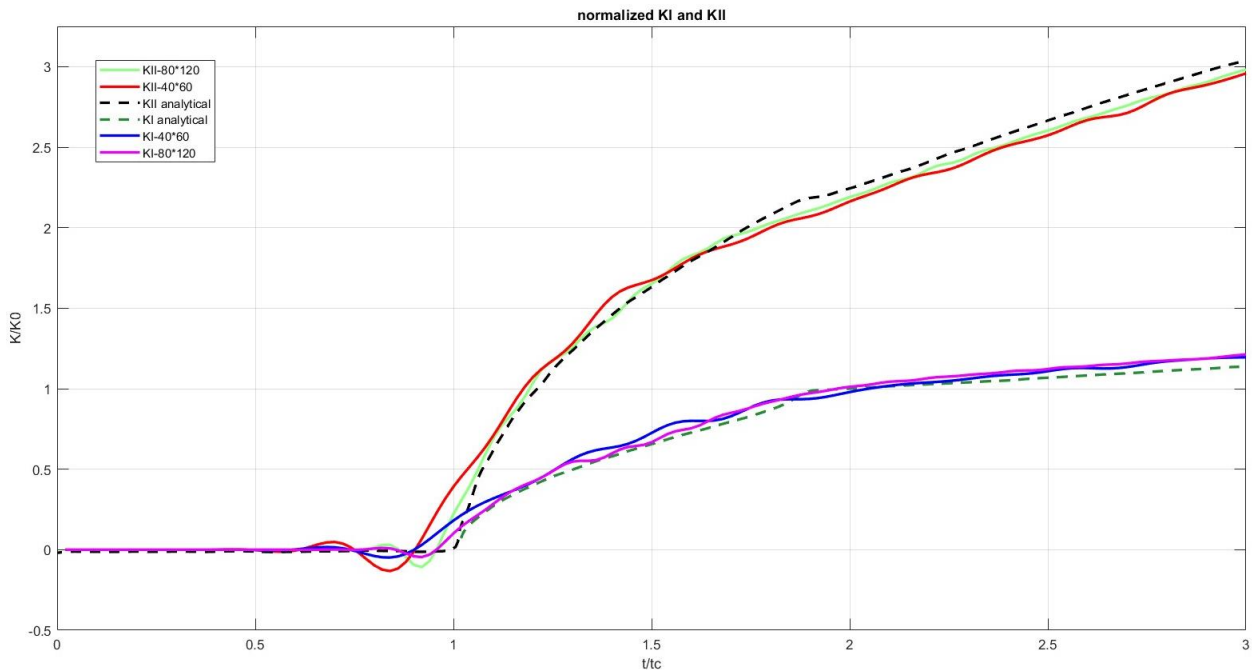


Figure 17-Normalized SIF plotted against normalized time for a stationary semi-infinite mixed-mode crack.

Based on Figure 17, the numerical outcomes exhibit a commendable concurrence with the analytical stress intensity factors. Moreover, it is evident that the outcomes remain consistent across various mesh configurations, affirming the adequacy of the candidate meshes in attaining convergence. So, the presented procedure and the M-integral formula demonstrate effective functionality.

3.4 Stationary and Moving Crack in Mode I

Now, it is necessary to validate the method for calculating the M_d integral in problems involving crack growth and validate the algorithm of the discontinuous Galerkin method and the balance recovery algorithm using a well-known example (Liu et al., 2011; Réthoré et al., 2005) of a propagating crack with a presumed speed, along with an analytical solution for the process (Freund, 1990). In this example, a plate with the geometry shown in Figure 18 is assumed to be subjected to tensile loading as a function of time, applied at its upper side.

The dimensions according to the figure are: $L=10$ m; $a=5$ m; $h=2$ m, and the material properties are defined in Table 4.

Table 4- Material properties

Young's modulus (GPa)	Poisson's ratio	Density(kg/m ³)
210	0.3	8000

Note that in the dynamic examples, the Rayleigh damping coefficients γ_k and γ_m are set to 0.001 and 0, respectively.

The external load is defined as follows:

$$P = \sigma_0 \begin{cases} t/(.2t_c) & 0 \leq t \leq .2t_c \\ 1 & t > .2t_c \end{cases} \quad (3-1)$$

Here, σ_0 is equal to 0.5 MPa, and t_c is the time it takes for a longitudinal wave to traverse half of the plate's height. This time is equal to $t_c = h/C_d$, where C_d is equal to 5944 m/s.

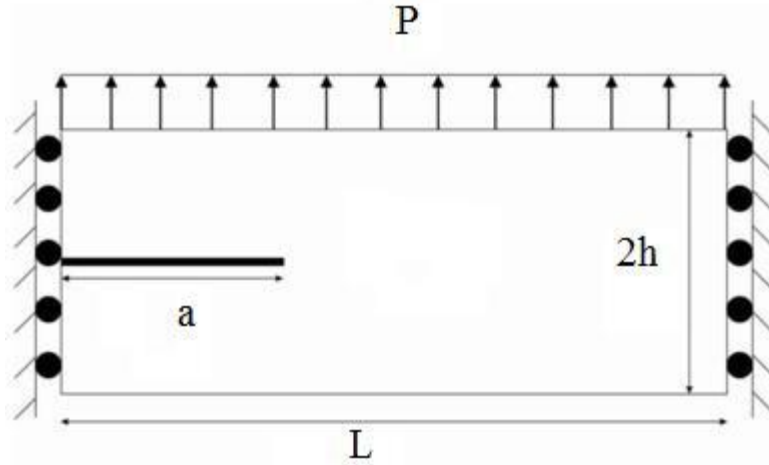


Figure 18-The geometry and boundary conditions for the discussed example

The crack velocity in this problem is assumed to be preset and is defined as follows:

$$V = \begin{cases} 0 & t \leq 1.5t_c \\ V_0 \sin\left(\frac{(t - 1.5t_c)\pi}{1.4t_c}\right) & 1.5t_c \leq t \leq 2.2t_c \\ V_0 & t \geq 2.2t_c \end{cases} \quad (3-2)$$

The analytical solution for this problem under uniform loading, as provided by (Freund, 1990), is presented as follows:

$$K_I^0(V_c, t) = K_I^0(0, t)\hat{k}(V_c) \quad (3-3)$$

Where $K_I^0(0, t)$ represents the stress intensity factor for a speed of zero and can be expressed as follows as soon as the tensile wave reaches the crack at t_c :

$$K_I^0(0, t) = \begin{cases} 0 & t < t_c \\ \frac{2\sigma_0}{1-\nu} \sqrt{\frac{C_d(t-t_c)(1-\nu)}{\pi}} & t \geq t_c \end{cases} \quad (3-4)$$

Furthermore, $\hat{k}(V_c)$ is defined as follows:

$$\hat{k}(V_c) = \frac{1 - \frac{V_c}{C_R}}{\sqrt{1 - \frac{V_c}{C_d}}} \quad (3-5)$$

Where C_R , is equal to 2947 m/s.

Certainly, considering that the loading in the example differs from the analytical solution, we can calculate the dynamic stress intensity factor for other loadings using the theory proposed by (Ravi-Chandar, 2004). This theory likely provides a framework for calculating dynamic stress intensity factors under various loading conditions or for cracks with different propagation behaviors (This may involve assessing factors such as crack size, crack shape, crack growth rate, and material properties).

$$K_I^n(0, t) = \int_{-\infty}^{\infty} K_I^0(0, t - \tau) \dot{f}_n(\tau) d\tau \quad (3-6)$$

Where K_I^0 is the stress intensity factor for uniform loading, and \dot{f}_n is the derivative of loadings with respect to time. By applying the integral formulation for the introduced loading, the dynamic stress intensity factor can be obtained.

$$\check{K}_I(0, t) = \frac{K_I(0, t)}{\alpha \sigma_0 \sqrt{H}} = \frac{2}{3} \sqrt{\frac{.2t_c}{t_c}} \begin{cases} \left(\frac{t}{.2t_c}\right)^{1.5} & 0 \leq t < .2t_c \\ \left(\frac{t}{.2t_c}\right)^{1.5} - \left(\frac{t}{.2t_c} - 1\right)^{1.5} & t \geq .2t_c \end{cases} \quad (3-7)$$

Where

$$\alpha = \frac{2}{1 - \nu} \sqrt{\frac{1 - 2\nu}{\pi}} \quad (3-8)$$

The analytical solution was provided for an infinite medium, so simulations are performed only up to a time of $3t_c$, where the first reflected wave from the boundary reaches the crack tip.

For modeling this problem, a regular mesh, discontinuous Galerkin time integration with a time step of $0.2t_c$, an integration path radius of M_d equal to 0.5m, along with a balance recovery algorithm, has been used. Additionally, among the provided equations for the Rayleigh wave speed, the following relationship was selected with minimum error.

$$C_{ksr} = C_s \times \left(\frac{d(1)}{d(2) + d(3) * v + d(4) * v^2 + d(5) * v^3 + d(6) * v^4 + d(7) * v^5} \right) \quad (3-9)$$

Where

$$d = [1; 1.14416; -0.25557; 0.10791; 0.04916; -0.03049; -0.0237]$$

To compare the results obtained with the numerical solution, results from (Liu et al., 2011), which is obtained using the spectral element method with a 120x60 mesh, is utilized. The results for the dynamic stress intensity factor are presented in Figure 19 (note that in all figures, time is non-dimensionalized with t_c and stress intensity factor with k_0 , equal to $\sigma_0\sqrt{H}$). As evident in the figure, the results obtained in this study show good agreement with the results from the analytical solution and the reference numerical solution. This confirms the accuracy of the M_d integral along with the auxiliary field used in the crack growth problem.

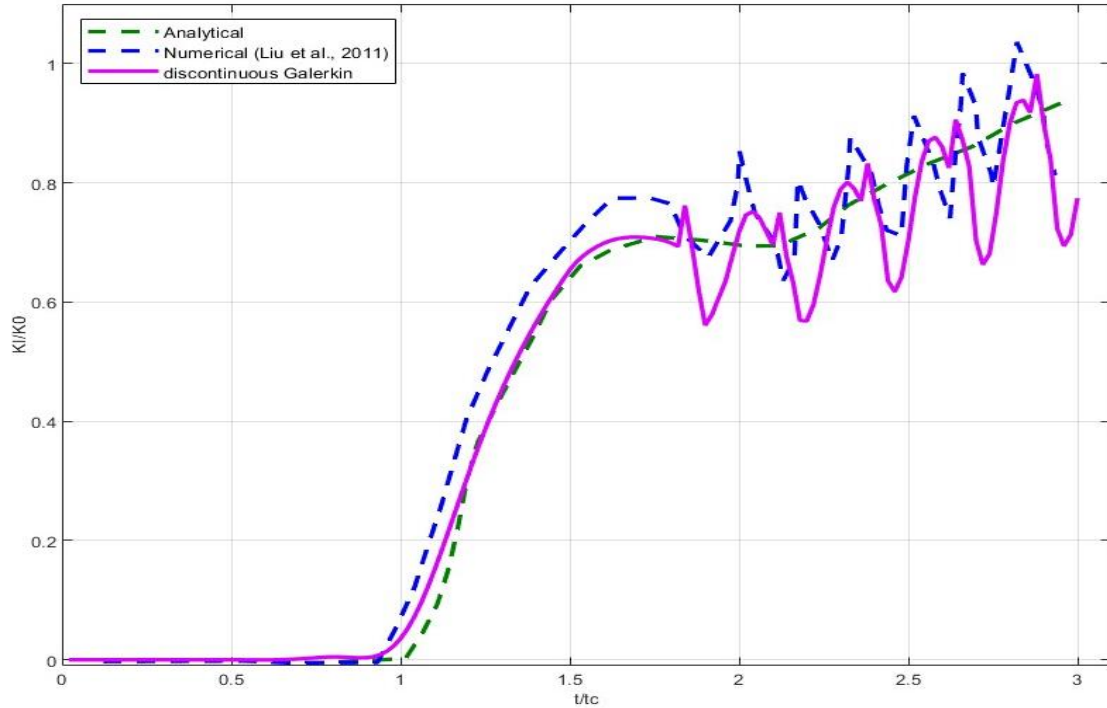


Figure 19- The dynamic stress intensity factor for the recommended mesh in the reference (Liu et al., 2011).

To evaluate the time integration method used, the example was solved using the Newmark method, and the results are presented in Figure 20. As evident from the figure, employing discontinuous Galerkin integration method significantly reduces the numerical oscillations compared to the Newmark method. While the Newmark integration works well as long as the crack remains static, it introduces oscillations in the numerical solution after crack growth initiation, which become more prominent over time. In an analysis where the crack propagation rate is not predetermined, these numerical oscillations make it challenging to predict quantities such as crack velocity, fracture energy, dynamic stress intensity factor, etc., accurately over time.

As explained before, the change in the crack tip elements and the appearance of new degrees of freedom disrupt the equilibrium at the beginning of each time step, leading to numerical oscillations. To demonstrate the impact of the balance recovery algorithm, the example was also solved without using this algorithm, and the results are presented in Figure 21 with discontinuous Galerkin time integration and in Figure 22 with Newmark integration.

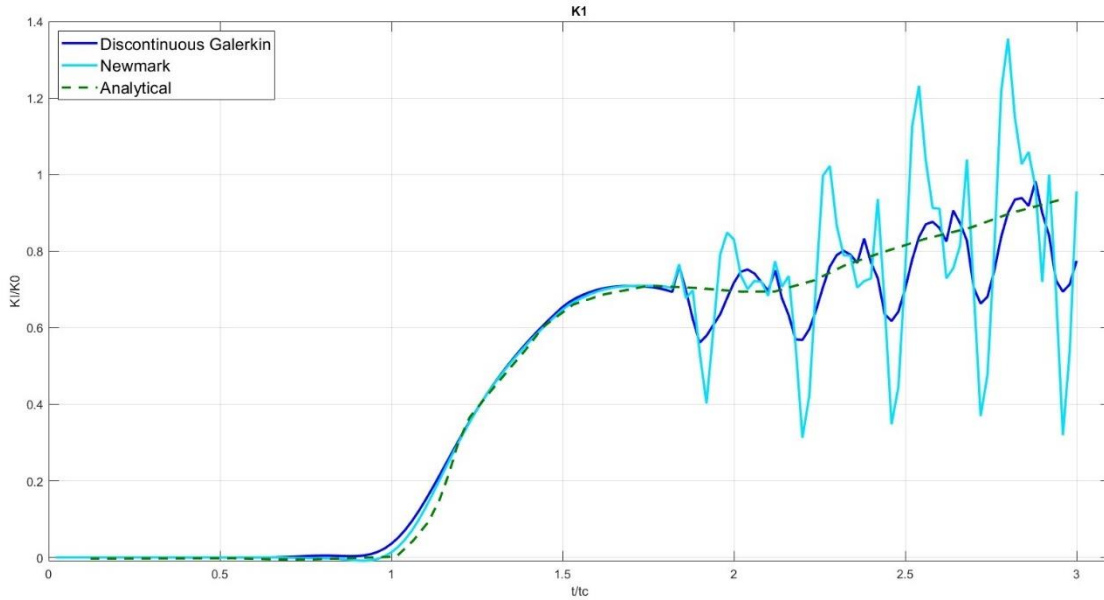


Figure 20- The analysis conducted in the study involved two different time integration methods: the discontinuous Galerkin time integration and the Newmark method.

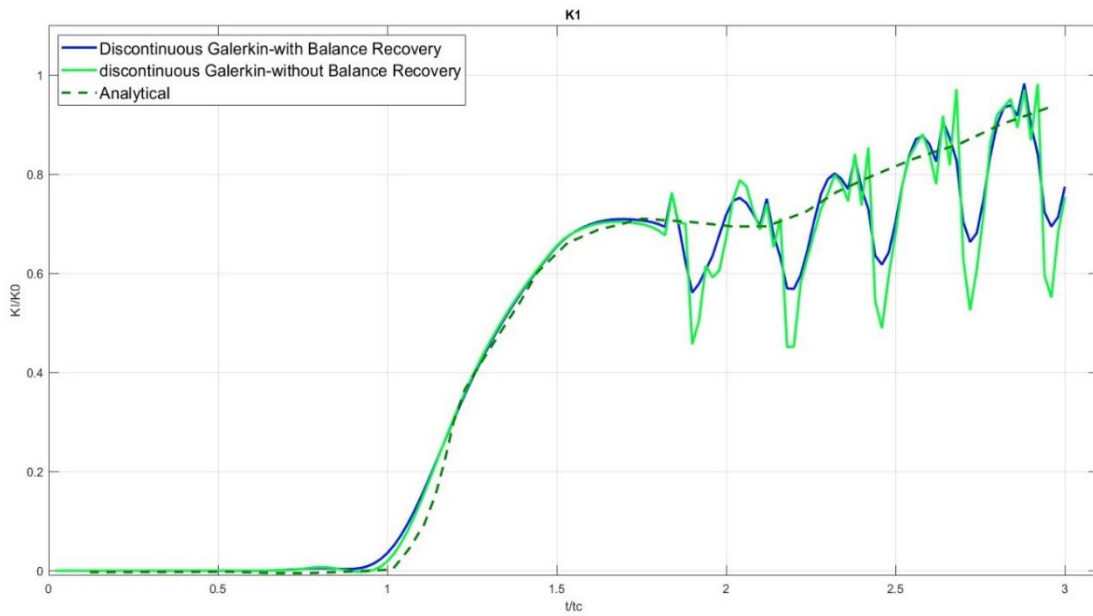


Figure 21- The inclusion of the balance-recovery algorithm along with the Discontinuous Galerkin (Edgerton & Barstow) time integration method has a significant impact on the numerical simulations.

The impact of the balance recovery algorithm on mitigating numerical oscillations is conspicuously evident in these configurations. Consequently, the utilization of this

algorithm, coupled with the discontinuous integration of the Galerkin method, appears imperative for attaining a fully stable solution.

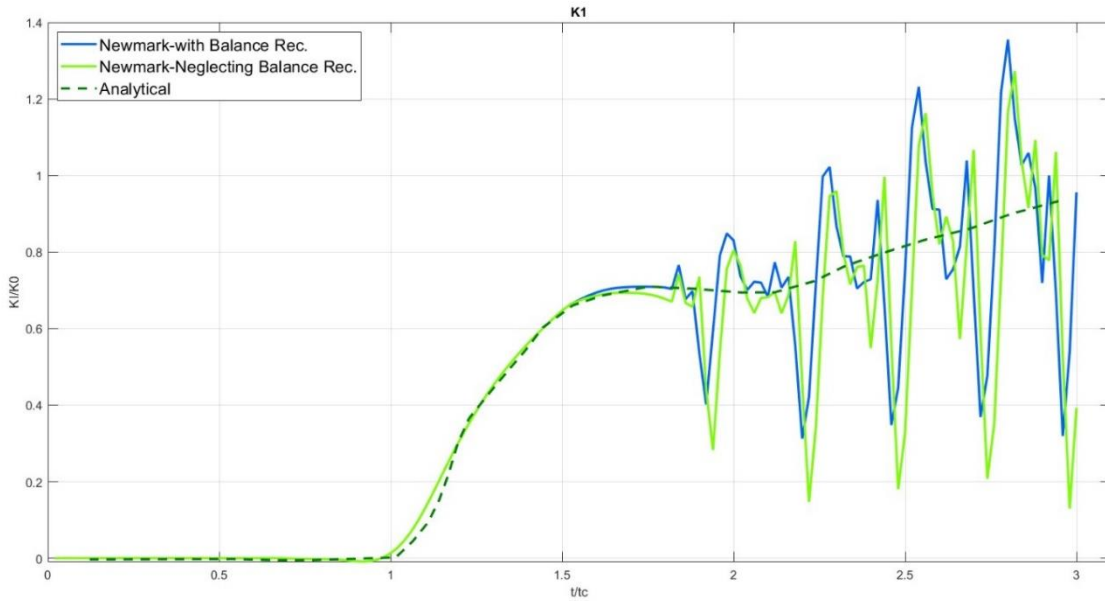


Figure 22- The influence of the balance recovery algorithm in conjunction with the Newmark integration method.

To investigate the effect of mesh refinement on the accuracy of results and the level of oscillations, an 80x40 mesh refinement scheme, as recommended in reference (Réthoré et al., 2005), is considered. It is compared with 20x40, 40x40, and 60x40 meshes, and the obtained results are depicted in Figure 23. As it becomes evident, increasing the mesh refinement in the horizontal direction leads to a reduction in the amplitude of oscillations, bringing the numerical solution closer to the analytical solution. However, it is noteworthy that for the 80x40 mesh refinement, the numerical solution exhibits a closer match to the analytical solution.

Furthermore, this reference mesh is compared with 80x20, 80x40, and 80x120 meshes, as illustrated in Figure 24. Again, Enhancing Vertical mesh refinement reduces oscillation amplitudes, aligning the numerical solution more closely with the analytical one.

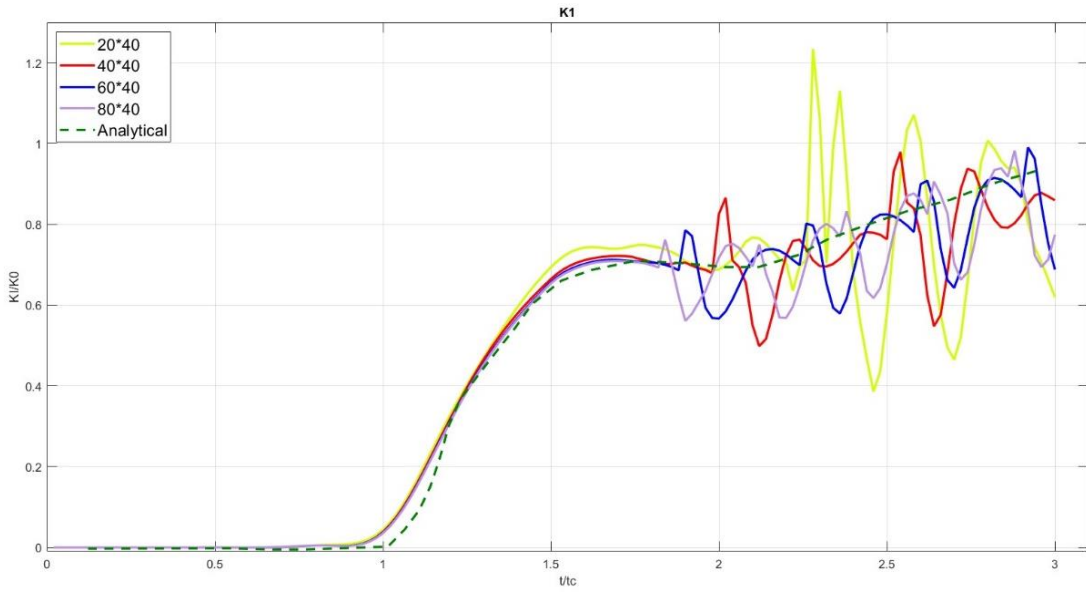


Figure 23- The Effect of Mesh Refinement in the Horizontal Direction

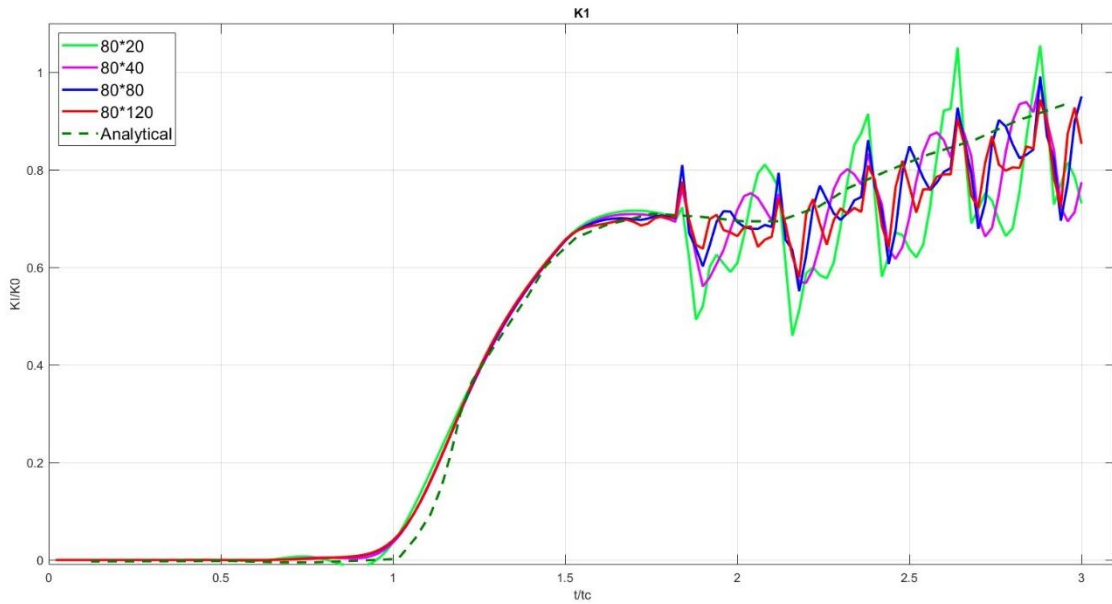


Figure 24-The Effect of Mesh Refinement in the Vertical Direction

Considering the outcomes of the comparison between mesh refinement in two different directions, it is likely that the optimal solution lies within a structured mesh that conforms to the problem's geometry. In this regard, three mesh refinements, 40x40, 80x80, and

160x160, are compared in Figure 25. As evident, by maintaining this pattern and reducing the mesh size, a solution with significantly reduced oscillations can be achieved.

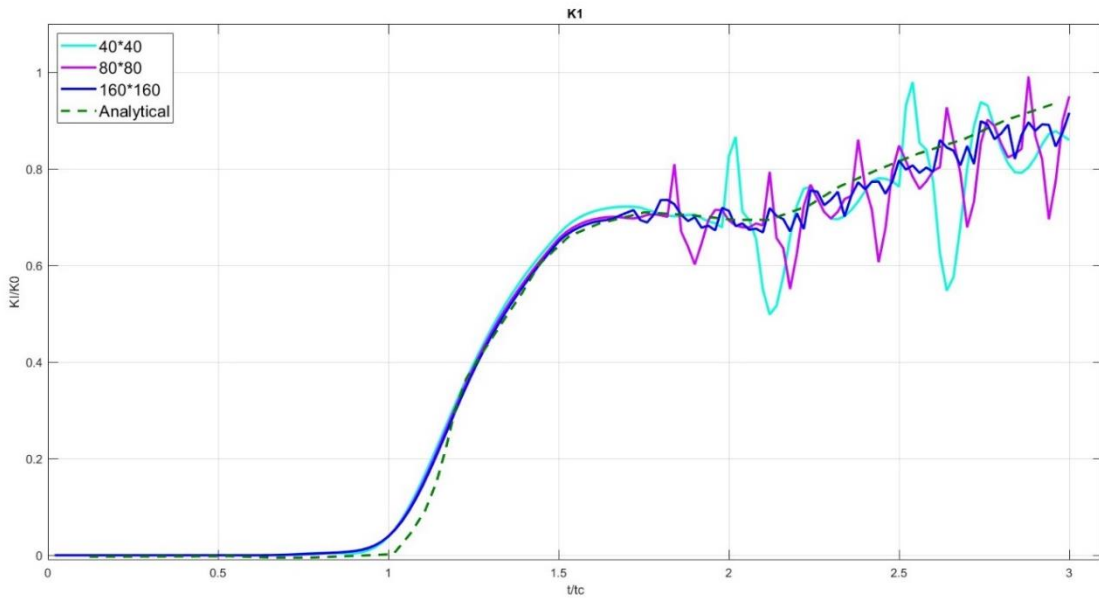


Figure 25- Comparison of Mesh Refinement with Equal Division in Horizontal and Vertical Directions

Furthermore, to investigate the effect of the time step in the analysis, time steps of $5\mu\text{s}$ and $80\mu\text{s}$ are compared with a time step of $20\mu\text{s}$ in Figure 26. As demonstrated, a time step of $80\mu\text{s}$ allows for a solution with minimal oscillations, although long time intervals do not permit the accurate determination of the initial crack location within the time intervals.

As depicted in Figure 27, it can be observed that by reducing the radius of the M_d integral, the amplitude of oscillations has slightly decreased. So, even a radius equal to $0.9\text{E}3$ may be enough for our calculations.

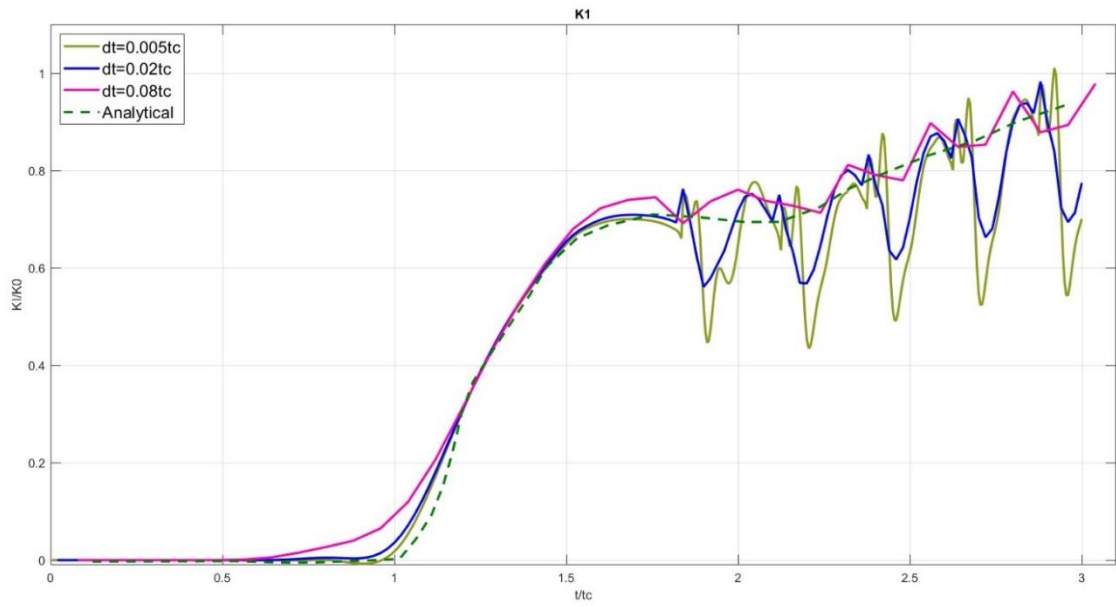


Figure 26- Comparison of Different Time Steps.

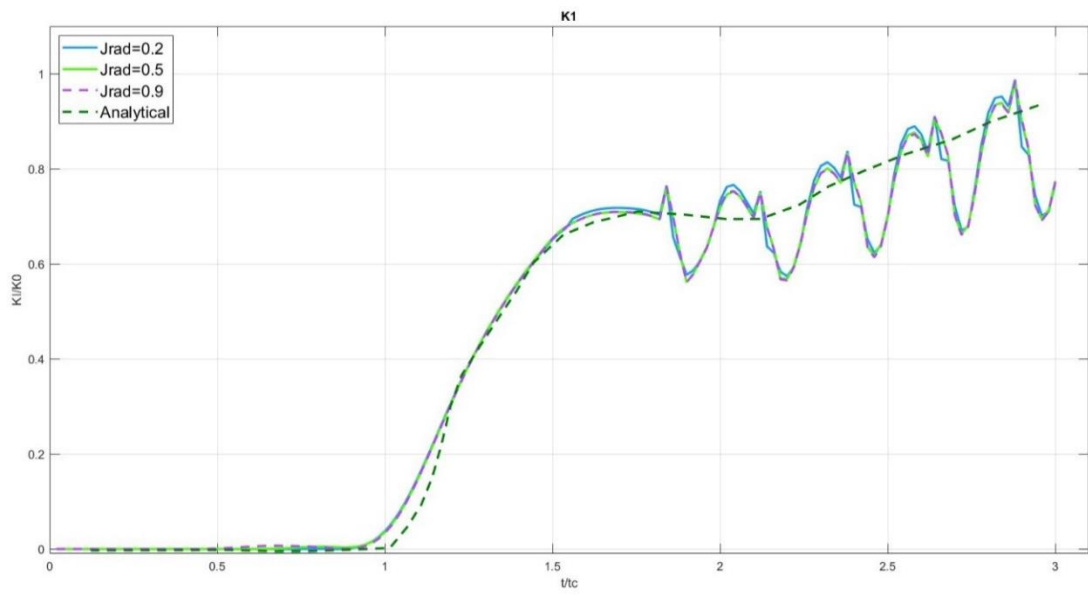


Figure 27- Comparison of Various Radii for the M_d Integral

Ultimately, this specific example was resolved using an irregular mesh, with iso-parametric and sub-parametric elements. To highlight the irregular structure of the mesh, a segment of it is depicted in Figure 28.

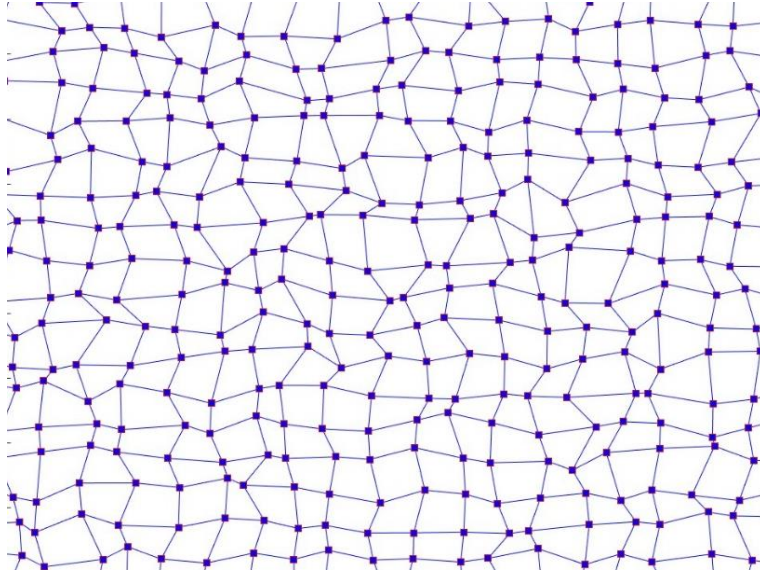


Figure 28- A snapshot of the non-uniform mesh utilized in this example.

In the figures presented below, a comparison is made between the stress intensity factor obtained for the non-uniform mesh using iso-parametric and sub-parametric elements and the SIF values calculated for the uniform mesh. As illustrated in Figure 29, when the mesh is non-uniform, there is an increase in oscillations. However, in the case of a non-uniform mesh, a comparison of the results obtained from iso-parametric and sub-parametric elements reveals a decrease in oscillations when using sub-parametric element (Figure 30).

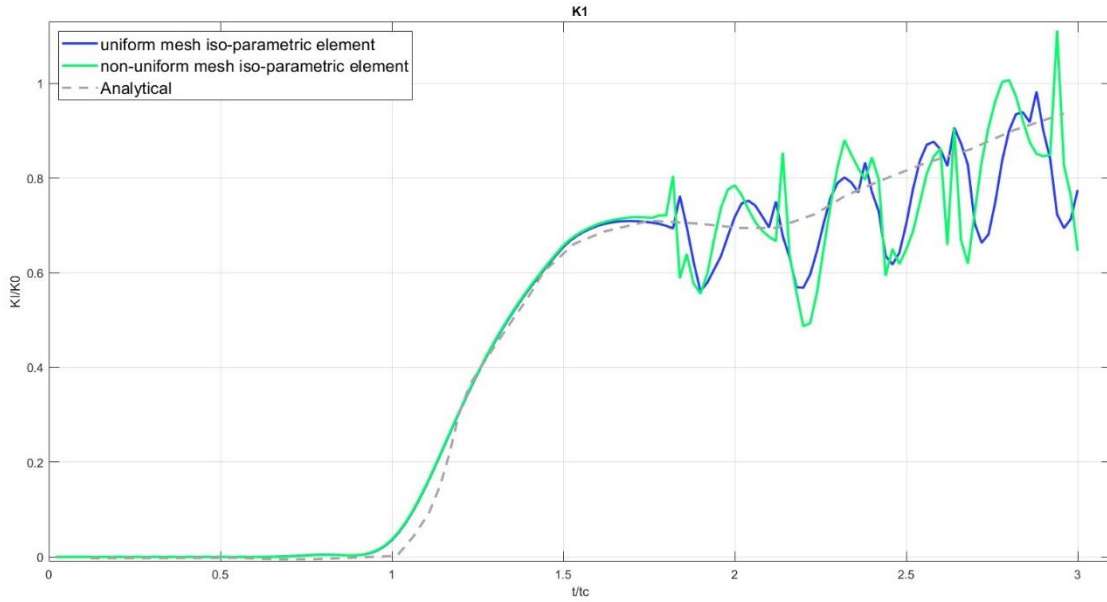


Figure 29- A comparison of the Stress Intensity Factors with the uniform and non-uniform meshes.

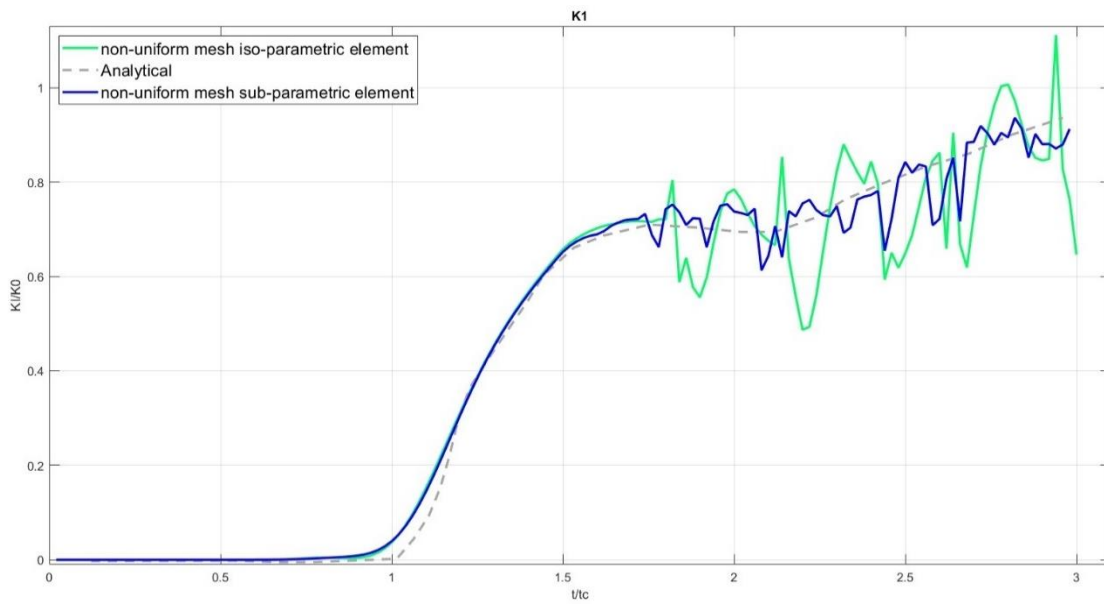


Figure 30- A comparison of the Stress Intensity Factors with sub-parametric and iso-parametric elements

4 Conclusion and Suggestions

4.1 Conclusion

In summary, this thesis has underscored the critical importance of accurate and stable numerical analysis in the context of dynamic crack growth, which finds application in various crucial sectors such as the Aerospace Industry, Structural Engineering, Materials Testing, Oil and Gas Industry, and Biomechanics. Among these applications, some require irregular mesh definitions. For instance, anisotropic materials like polycrystals with multiple crystal grains benefit from non-uniform meshes to align mesh elements with material properties, leading to more accurate simulations. Irregular meshes are also valuable in cases of large deformation and contact problems, helping to adapt to changes in geometry and surface interactions.

The central inquiry of this thesis revolved around enhancing the accuracy of stress intensity factor calculations in the presence of irregular meshes. Several significant findings and methodologies have been presented:

First, the utilization of the Discontinuous Galerkin method for temporal integration was shown to be highly effective, reducing oscillations during crack propagation in comparison to the traditional Newmark method. This choice of integration method has the potential to significantly improve the reliability of simulations.

Furthermore, the thesis emphasized the issue of residual forces generated as cracks extend, which can disturb the stability of numerical solutions. The implementation of a balance recovery algorithm was demonstrated as a pivotal means of mitigating these destabilizing forces and thereby enhancing solution stability.

The study also revealed the influence of time intervals on oscillations, highlighting that a reduction in the time interval can lead to decreased oscillations. This insight has practical implications for refining the temporal discretization in such simulations.

In terms of mesh characteristics, the thesis illustrated that increasing mesh divisions in both directions can effectively reduce oscillations. Uniform mesh divisions in both directions were found to be particularly advantageous in minimizing oscillations, underscoring the importance of mesh design.

Sensitivity analyses were established as a fundamental practice to ensure numerical convergence in interaction integral results. Gradually increasing the interaction integral radius, guided by the mesh density, is essential. This practice enables researchers to fine-tune the radius to align with the level of mesh refinement, thereby ensuring more accurate calculations.

Finally, for cases involving irregular meshes, the strategic use of 4-node elements for field variable discretization and 3-node elements for geometry discretization was advocated. This approach, promoting a constant Jacobian over elements, offers a solution that minimizes errors in the outcomes of dynamic crack growth simulations.

In closing, this thesis represents a significant contribution to the field of dynamic crack growth analysis. The methodologies and findings presented here serve as valuable tools for researchers seeking to conduct precise and stable numerical analyses in the presence of irregular meshes, ultimately advancing the reliability and accuracy of dynamic crack growth simulations in real-world applications.

4.2 Suggestions

This thesis has opened several avenues for future investigations in the field of dynamic crack growth analysis. To continue building upon the findings and methodologies presented in this study, the following suggestions are provided:

- Considering dynamic auxiliary stress and strain field in interaction integral
- Considering dynamic enrichment function for crack tip
- Considering multi-material or composite structures, which are prevalent in aerospace and structural engineering, and investigate the impact of irregular meshes on crack growth in such heterogeneous systems.
- Develop three-dimensional crack propagation.
- Develop the algorithm to model the materials exhibiting significant nonlinearity and viscoelastic behavior, which is common in biomechanics and certain industrial materials.

5 References

- Achenbach, J. D., & Bazant, Z. P. (1975). Elastodynamic near-tip stress and displacement fields for rapidly propagating cracks in orthotropic materials.
- Achenbach, J. J. M. t. (1972). Dynamic effects in brittle fracture. *I*, 1-57.
- Agathos, K., Ventura, G., Chatzi, E., & Bordas, S. P. A. (2018). Stable 3D XFEM/vector level sets for non-planar 3D crack propagation and comparison of enrichment schemes. *113*(2), 252-276. <https://doi.org/https://doi.org/10.1002/nme.5611>
- Amiri, F., Anitescu, C., Arroyo, M., Bordas, S. P. A., & Rabczuk, T. J. C. M. (2014). XLME interpolants, a seamless bridge between XFEM and enriched meshless methods. *53*, 45-57.
- Asadpoure, A., Mohammadi, S., & Vafai, A. J. T.-W. S. (2006). Crack analysis in orthotropic media using the extended finite element method. *44*(9), 1031-1038.
- Asadpoure, A., & Mohammadi, S. J. I. J. f. N. M. i. E. (2007). Developing new enrichment functions for crack simulation in orthotropic media by the extended finite element method. *69*(10), 2150-2172.
- Ayhan, A. O., & Nied, H. J. I. j. f. n. m. i. e. (2002). Stress intensity factors for three-dimensional surface cracks using enriched finite elements. *54*(6), 899-921.
- Baker, B. (1962). Dynamic stresses created by a moving crack.
- Baydoun, M., & Fries, T. J. I. j. o. f. (2012). Crack propagation criteria in three dimensions using the XFEM and an explicit–implicit crack description. *178*, 51-70.
- Belytschko, T., & Black, T. J. I. j. f. n. m. i. e. (1999). Elastic crack growth in finite elements with minimal remeshing. *45*(5), 601-620.
- Belytschko, T., Chen, H., Xu, J., & Zi, G. J. I. j. f. n. m. i. e. (2003). Dynamic crack propagation based on loss of hyperbolicity and a new discontinuous enrichment. *58*(12), 1873-1905.

- Belytschko, T., & Chen, H. J. I. J. o. C. M. (2004). Singular enrichment finite element method for elastodynamic crack propagation. *I(01)*, 1-15.
- Belytschko, T., Gracie, R., Ventura, G. J. M., Science, S. i. M., & Engineering. (2009). A review of extended/generalized finite element methods for material modeling. *17(4)*, 043001.
- Benvenuti, E., Tralli, A., & Ventura, G. J. I. J. f. N. M. i. E. (2008). A regularized XFEM model for the transition from continuous to discontinuous displacements. *74(6)*, 911-944.
- Benvenuti, E., Ventura, G., & Ponara, N. J. A. (2012). Finite element quadrature of regularized discontinuous and singular level set functions in 3D problems. *5(4)*, 529-544.
- Bordas, S. P., Natarajan, S., Kerfriden, P., Augarde, C. E., Mahapatra, D. R., Rabczuk, T., & Pont, S. D. J. I. J. f. N. M. i. E. (2011). On the performance of strain smoothing for quadratic and enriched finite element approximations (XFEM/GFEM/PUFEM). *86(4-5)*, 637-666.
- Bordas, S. P., Rabczuk, T., Hung, N.-X., Nguyen, V. P., Natarajan, S., Bog, T., . . . structures. (2010). Strain smoothing in FEM and XFEM. *88(23-24)*, 1419-1443.
- Budyn, E., Zi, G., Moës, N., & Belytschko, T. J. I. j. f. n. m. i. e. (2004). A method for multiple crack growth in brittle materials without remeshing. *61(10)*, 1741-1770.
- Byfut, A., & Schröder, A. J. I. j. f. n. m. i. e. (2012). hp-adaptive extended finite element method. *89(11)*, 1392-1418.
- Chahine, E., Laborde, P., & Renard, Y. J. A. N. M. (2011). A non-conformal eXtended Finite Element approach: Integral matching Xfem. *61(3)*, 322-343.
- Chen, E. (1978). Sudden appearance of a crack in a stretched finite strip.
- Cheng, K.-W., Fries, T.-P. J. C. M. i. A. M., & Engineering. (2012). XFEM with hanging nodes for two-phase incompressible flow. *245*, 290-312.

- Chessa, J., Belytschko, T. J. C. M. i. A. M., & Engineering. (2006). A local space–time discontinuous finite element method. *195*(13-16), 1325-1343.
- Chessa, J., & Belytschko, T. J. I. J. f. N. M. i. E. (2004). Arbitrary discontinuities in space–time finite elements by level sets and X-FEM. *61*(15), 2595-2614.
- Chessa, J., Wang, H., & Belytschko, T. J. I. J. f. N. M. i. E. (2003). On the construction of blending elements for local partition of unity enriched finite elements. *57*(7), 1015-1038.
- Combesure, A., Gravouil, A., Grégoire, D., Réthoré, J. J. C. M. i. A. M., & Engineering. (2008). X-FEM a good candidate for energy conservation in simulation of brittle dynamic crack propagation. *197*(5), 309-318.
- Cotterell, B. (1964). On the nature of moving cracks.
- Craggs, J. W. J. J. o. t. M., & Solids, P. o. (1960). On the propagation of a crack in an elastic-brittle material. *8*(1), 66-75.
- Dally, J. W. (1987). Dynamic photoelasticity and its application to stress wave propagation, fracture mechanics and fracture control. In *Static and Dynamic Photoelasticity and Caustics: Recent Developments* (pp. 247-406). Springer.
- Daux, C., Moës, N., Dolbow, J., Sukumar, N., & Belytschko, T. J. I. j. f. n. m. i. e. (2000). Arbitrary branched and intersecting cracks with the extended finite element method. *48*(12), 1741-1760.
- Dolbow, J., Moës, N., Belytschko, T. J. C. m. i. a. M., & engineering. (2001). An extended finite element method for modeling crack growth with frictional contact. *190*(51-52), 6825-6846.
- Dolbow, J., Moës, N., Belytschko, T. J. F. e. i. a., & design. (2000). Discontinuous enrichment in finite elements with a partition of unity method. *36*(3-4), 235-260.
- Dolbow, J. E. (1999). *An extended finite element method with discontinuous enrichment for applied mechanics*. Northwestern university.
- Edgerton, H., & Barstow, F. J. J. o. t. A. C. S. (1941). Further Studies of Glass Fracture with High-Speed Photography. *24*(4), 131-137.

- Elguedj, T., Gravouil, A., Maigre, H. J. C. M. i. A. M., & Engineering. (2009). An explicit dynamics extended finite element method. Part 1: mass lumping for arbitrary enrichment functions. *198*(30-32), 2297-2317.
- Eсна Ashari, S., & Mohammadi, S. J. J. o. c. m. (2012). Fracture analysis of FRP-reinforced beams by orthotropic XFEM. *46*(11), 1367-1389.
- Fleming, M., Chu, Y., Moran, B., & Belytschko, T. J. I. j. f. n. m. i. e. (1997). Enriched element-free Galerkin methods for crack tip fields. *40*(8), 1483-1504.
- Freund, L. (1976). Dynamic Crack Propagation in Brittle Solids. Report of the Workshop on Application of Elastic Waves in Electrical Waves in Electrical Devices, Non-Destructive Testing and Seismology: Held at Northwestern University, May 24-26, 1976,
- Freund, L., & Clifton, R. J. J. o. e. (1974). On the uniqueness of plane elastodynamic solutions for running cracks. *4*(4), 293-299.
- Freund, L., Douglas, A. J. J. o. t. M., & Solids, P. o. (1982). The influence of inertia on elastic-plastic antiplane-shear crack growth. *30*(1-2), 59-74.
- Freund, L. B. (1998). *Dynamic fracture mechanics*. Cambridge university press.
- Freund, L. J. N. Y. (1990). *Dynamic fracture mechanics* cambridge university press.
- Fries, T. P., & Baydoun, M. J. I. J. f. n. m. i. e. (2012). Crack propagation with the extended finite element method and a hybrid explicit–implicit crack description. *89*(12), 1527-1558.
- Fries, T. P., & Belytschko, T. J. I. j. f. n. m. i. e. (2006). The intrinsic XFEM: a method for arbitrary discontinuities without additional unknowns. *68*(13), 1358-1385.
- Fries, T. P., & Belytschko, T. J. I. j. f. n. m. i. e. (2010). The extended/generalized finite element method: an overview of the method and its applications. *84*(3), 253-304.
- Fries, T. P., & Zilian, A. J. I. J. f. N. M. i. E. (2009). On time integration in the XFEM. *79*(1), 69-93.

- Fries, T. P. J. I. J. f. N. M. i. E. (2008). A corrected XFEM approximation without problems in blending elements. *75*(5), 503-532.
- Gao, H., Klein, P. J. J. o. t. M., & Solids, P. o. (1998). Numerical simulation of crack growth in an isotropic solid with randomized internal cohesive bonds. *46*(2), 187-218.
- González-Albuixech, V. F., Giner, E., Tarancón, J. E., Fuenmayor, F. J., Gravouil, A. J. C. m. i. a. m., & engineering. (2013). Domain integral formulation for 3-D curved and non-planar cracks with the extended finite element method. *264*, 129-144.
- González-Albuixech, V. F., Giner, E., Tarancon, J. E., Fuenmayor, F. J., & Gravouil, A. J. I. J. f. N. M. i. E. (2013). Convergence of domain integrals for stress intensity factor extraction in 2-D curved cracks problems with the extended finite element method. *94*(8), 740-757.
- Gracie, R., Wang, H., & Belytschko, T. J. I. J. f. N. M. i. E. (2008). Blending in the extended finite element method by discontinuous Galerkin and assumed strain methods. *74*(11), 1645-1669.
- Gravouil, A., Elguedj, T., Maigre, H. J. C. M. i. A. M., & Engineering. (2009). An explicit dynamics extended finite element method. Part 2: Element-by-element stable-explicit/explicit dynamic scheme. *198*(30-32), 2318-2328.
- Grégoire, D., Maigre, H., Rethore, J., Combescure, A. J. I. j. o. s., & structures. (2007). Dynamic crack propagation under mixed-mode loading—comparison between experiments and X-FEM simulations. *44*(20), 6517-6534.
- Kalthoff, J. F. (1987). The shadow optical method of caustics. In *Static and Dynamic Photoelasticity and Caustics: Recent Developments* (pp. 407-522). Springer.
- Kanninen, M., Popelar, C., & Saunders, H. (1988). *Advanced fracture mechanics*.
- Kerckhof, F. (1973). General Lecture Wave fractographic investigations of brittle fracture dynamics. Proceedings of an international conference on Dynamic Crack Propagation,
- Khoei, A. R. (2015). *Extended Finite Element Method: Theory and Applications*. Wiley. <https://books.google.it/books?id=unKwCQAAQBAJ>

- Kim, J.-H., Paulino, G. H. *J. I. j. o. s., & structures.* (2003). The interaction integral for fracture of orthotropic functionally graded materials: evaluation of stress intensity factors. *40*(15), 3967-4001.
- Kirkaldy, D. J. G. K. (1863). *Experiments on Wrought Iron and Steel.*
- Laborde, P., Pommier, J., Renard, Y., & Salaün, M. *J. I. j. f. n. m. i. e.* (2005). High-order extended finite element method for cracked domains. *64*(3), 354-381.
- Lee, Y., & Freund, L. (1990). Fracture initiation due to asymmetric impact loading of an edge cracked plate.
- Legay, A., Wang, H., & Belytschko, T. *J. I. J. f. N. M. i. E.* (2005). Strong and weak arbitrary discontinuities in spectral finite elements. *64*(8), 991-1008.
- Legrain, G., Allais, R., & Cartraud, P. *J. I. J. f. N. M. i. E.* (2011). On the use of the extended finite element method with quadtree/octree meshes. *86*(6), 717-743.
- Legrain, G., Moes, N., & Verron, E. *J. I. J. f. N. M. i. E.* (2005). Stress analysis around crack tips in finite strain problems using the extended finite element method. *63*(2), 290-314.
- Li, F. Z., Shih, C. F., & Needleman, A. *J. E. f. m.* (1985). A comparison of methods for calculating energy release rates. *21*(2), 405-421.
- Li, X., Yao, D., & Lewis, R. *J. I. J. f. N. M. i. E.* (2003). A discontinuous Galerkin finite element method for dynamic and wave propagation problems in non-linear solids and saturated porous media. *57*(12), 1775-1800.
- Liu, Z., Menouillard, T., & Belytschko, T. *J. I. J. o. F.* (2011). An XFEM/Spectral element method for dynamic crack propagation. *169*, 183-198.
- Loehnert, S., & Belytschko, T. *J. I. J. o. F.* (2007). Crack shielding and amplification due to multiple microcracks interacting with a macrocrack. *145*, 1-8.
- Loehnert, S., Mueller-Hoeppe, D., & Wriggers, P. *J. I. J. f. N. M. i. E.* (2011). 3D corrected XFEM approach and extension to finite deformation theory. *86*(4-5), 431-452.

- Malischewsky, P. G. J. N. (2005). Comparison of approximated solutions for the phase velocity of Rayleigh waves (Comment on ‘Characterization of surface damage via surface acoustic waves’). *16*(6), 995.
- Manogg, P. J. I. J. o. F. M. (1966). Investigation of the rupture of a plexiglas plate by means of an optical method involving high-speed filming of the shadows originating around holes drilled in the plate. *2*, 604-613.
- Melenk, J. M., Babuška, I. J. C. m. i. a. m., & engineering. (1996). The partition of unity finite element method: basic theory and applications. *139*(1-4), 289-314.
- Menk, A., & Bordas, S. P. J. I. J. f. N. M. i. E. (2011). A robust preconditioning technique for the extended finite element method. *85*(13), 1609-1632.
- Menouillard, T., & Belytschko, T. J. A. m. (2010). Dynamic fracture with meshfree enriched XFEM. *213*(1-2), 53-69.
- Menouillard, T., & Belytschko, T. J. I. J. f. N. M. i. E. (2010). Smoothed nodal forces for improved dynamic crack propagation modeling in XFEM. *84*(1), 47-72.
- Menouillard, T., Rethore, J., Combescure, A., & Bung, H. J. I. J. f. N. M. i. E. (2006). Efficient explicit time stepping for the eXtended Finite Element Method (X-FEM). *68*(9), 911-939.
- Menouillard, T., Réthoré, J., Moës, N., Combescure, A., & Bung, H. J. I. J. f. N. M. i. E. (2008). Mass lumping strategies for X-FEM explicit dynamics: application to crack propagation. *74*(3), 447-474.
- Menouillard, T., Song, J.-H., Duan, Q., & Belytschko, T. J. I. J. o. F. (2010). Time dependent crack tip enrichment for dynamic crack propagation. *162*, 33-49.
- Minnebo, H. J. I. J. f. N. M. i. E. (2012). Three-dimensional integration strategies of singular functions introduced by the XFEM in the LEFM. *92*(13), 1117-1138.
- Moës, N., Béchet, E., & Tourbier, M. J. I. J. f. N. M. i. E. (2006). Imposing Dirichlet boundary conditions in the extended finite element method. *67*(12), 1641-1669.

- Moës, N., Dolbow, J., & Belytschko, T. J. I. j. f. n. m. i. e. (1999). A finite element method for crack growth without remeshing. *46*(1), 131-150.
- Moës, N., Gravouil, A., & Belytschko, T. J. I. j. f. n. m. i. e. (2002). Non-planar 3D crack growth by the extended finite element and level sets—Part I: Mechanical model. *53*(11), 2549-2568.
- Mohammadi, S. (2008). *Extended Finite Element Method: for Fracture Analysis of Structures*. Wiley. <https://books.google.it/books?id=I1thr8rgWQ8C>
- Mohammadi, S. (2012). *XFEM Fracture Analysis of Composites*. Wiley. <https://books.google.it/books?id=ygN21VdMrUEC>
- Motamedi, D., & Mohammadi, S. J. E. F. M. (2010). Dynamic analysis of fixed cracks in composites by the extended finite element method. *77*(17), 3373-3393.
- Motamedi, D., & Mohammadi, S. J. I. j. o. f. (2010). Dynamic crack propagation analysis of orthotropic media by the extended finite element method. *161*, 21-39.
- Motamedi, D., & Mohammadi, S. J. I. J. o. M. S. (2012). Fracture analysis of composites by time independent moving-crack orthotropic XFEM. *54*(1), 20-37.
- Mousavi, S., Grinspun, E., & Sukumar, N. J. I. J. f. N. M. i. E. (2011a). Harmonic enrichment functions: A unified treatment of multiple, intersecting and branched cracks in the extended finite element method. *85*(10), 1306-1322.
- Mousavi, S., Grinspun, E., & Sukumar, N. J. I. J. f. N. M. i. E. (2011b). Higher-order extended finite elements with harmonic enrichment functions for complex crack problems. *86*(4-5), 560-574.
- Mousavi, S., Sukumar, N. J. C. M. i. A. M., & Engineering. (2010). Generalized Gaussian quadrature rules for discontinuities and crack singularities in the extended finite element method. *199*(49-52), 3237-3249.
- Nakamura, T., Kushner, A., Lo, C. J. I. j. o. s., & structures. (1995). Interlaminar dynamic crack propagation. *32*(17-18), 2657-2675.
- Nicaise, S., Renard, Y., & Chahine, E. J. I. J. f. N. M. i. E. (2011). Optimal convergence analysis for the extended finite element method. *86*(4-5), 528-548.

- Nilsson, F. J. J. o. E. (1974). A note on the stress singularity at a non-uniformly moving crack tip. *4*(1), 73-75.
- Nishioka, T., & Atluri, S. J. E. F. M. (1983). Path-independent integrals, energy release rates, and general solutions of near-tip fields in mixed-mode dynamic fracture mechanics. *18*(1), 1-22.
- Nishioka, T., & Atluri, S. J. E. F. M. (1984). On the computation of mixed-mode K-factors for a dynamically propagating crack, using path-independent integrals J^k . *20*(2), 193-208.
- Nishioka, T., & Atluri, S. N. (1980). Numerical modeling of dynamic crack propagation in finite bodies, by moving singular elements—part 1: Formulation.
- Nistor, I., Pantalé, O., & Caperaa, S. J. A. i. E. S. (2008). Numerical implementation of the extended finite element method for dynamic crack analysis. *39*(7), 573-587.
- Oliver, J., Huespe, A. E., Pulido, M., & Samaniego, E. J. I. J. f. N. M. i. E. (2003). On the strong discontinuity approach in finite deformation settings. *56*(7), 1051-1082.
- Panetier, J., Ladeveze, P., & Chamoin, L. J. I. J. f. N. M. i. E. (2010). Strict and effective bounds in goal-oriented error estimation applied to fracture mechanics problems solved with XFEM. *81*(6), 671-700.
- Park, K., Pereira, J. P., Duarte, C. A., & Paulino, G. H. J. I. J. f. N. M. i. E. (2009). Integration of singular enrichment functions in the generalized/extended finite element method for three-dimensional problems. *78*(10), 1220-1257.
- Pathak, H., Singh, A., Singh, I. V., & Yadav, S. K. J. I. J. o. F. (2013). A simple and efficient XFEM approach for 3-D cracks simulations. *181*, 189-208.
- Peerlings, R. d., De Borst, R., Brekelmans, W., & Geers, M. J. E. J. o. M.-A. S. (2002). Localisation issues in local and nonlocal continuum approaches to fracture. *21*(2), 175-189.
- Prange, C., Loehnert, S., & Wriggers, P. J. I. J. f. N. M. i. E. (2012). Error estimation for crack simulations using the XFEM. *91*(13), 1459-1474.

- Rahman, M., & Michelitsch, T. J. W. m. (2006). A note on the formula for the Rayleigh wave speed. *43*(3), 272-276.
- Ravi-Chandar, K. (2004). *Dynamic fracture*. Elsevier.
- Réthoré, J., Gravouil, A., Combescure, A. J. C. m. i. a. m., & engineering. (2004). A stable numerical scheme for the finite element simulation of dynamic crack propagation with remeshing. *193*(42-44), 4493-4510.
- Réthoré, J., Gravouil, A., & Combescure, A. J. I. J. f. n. m. i. E. (2005). A combined space–time extended finite element method. *64*(2), 260-284.
- Rice, J. R. (1968). A path independent integral and the approximate analysis of strain concentration by notches and cracks.
- Rice, J. R. J. F. a. a. t. (1968). Mathematical analysis in the mechanics of fracture. *2*, 191-311.
- Richardson, C. L., Hegemann, J., Sifakis, E., Hellrung, J., & Teran, J. M. J. I. J. f. N. M. i. E. (2011). An XFEM method for modeling geometrically elaborate crack propagation in brittle materials. *88*(10), 1042-1065.
- Ródenas, J. J., González-Estrada, O. A., Díez, P., Fuenmayor, F. J. J. C. M. i. A. M., & Engineering. (2010). Accurate recovery-based upper error bounds for the extended finite element framework. *199*(37-40), 2607-2621.
- Rodenas, J. J., González-Estrada, O. A., Fuenmayor, F. J., & Chinesta, F. J. C. M. (2013). Enhanced error estimator based on a nearly equilibrated moving least squares recovery technique for FEM and XFEM. *52*, 321-344.
- Ródenas, J. J., González-Estrada, O. A., Tarancón, J. E., & Fuenmayor, F. J. J. I. J. f. N. M. i. E. (2008). A recovery-type error estimator for the extended finite element method based on singular+ smooth stress field splitting. *76*(4), 545-571.
- Rüter, M., Gerasimov, T., & Stein, E. J. C. M. (2013). Goal-oriented explicit residual-type error estimates in XFEM. *52*(2), 361-376.

- Shen, Y., Lew, A. J. C. M. i. A. M., & Engineering. (2010). Stability and convergence proofs for a discontinuous-Galerkin-based extended finite element method for fracture mechanics. *199*(37-40), 2360-2382.
- Shen, Y., & Lew, A. J. I. j. f. n. m. i. e. (2010). An optimally convergent discontinuous Galerkin-based extended finite element method for fracture mechanics. *82*(6), 716-755.
- Shibanuma, K., Utsunomiya, T. J. F. E. i. A., & Design. (2009). Reformulation of XFEM based on PUFEM for solving problem caused by blending elements. *45*(11), 806-816.
- Shibanuma, K., Utsunomiya, T. J. F. E. i. A., & Design. (2011). Evaluation on reproduction of priori knowledge in XFEM. *47*(4), 424-433.
- Stazi, F., Budyn, E., Chessa, J., & Belytschko, T. J. C. M. (2003). An extended finite element method with higher-order elements for curved cracks. *31*(1), 38-48.
- Stolarska, M., Chopp, D. L., Moës, N., & Belytschko, T. J. I. j. f. n. m. i. E. (2001). Modelling crack growth by level sets in the extended finite element method. *51*(8), 943-960.
- Sukumar, N., Chopp, D. L., Béchet, E., & Moës, N. J. I. j. f. n. m. i. e. (2008). Three-dimensional non-planar crack growth by a coupled extended finite element and fast marching method. *76*(5), 727-748.
- Tabarraei, A., Sukumar, N. J. C. M. i. A. M., & Engineering. (2008). Extended finite element method on polygonal and quadtree meshes. *197*(5), 425-438.
- Tarancón, J., Vercher, A., Giner, E., & Fuenmayor, F. J. I. J. f. N. M. i. E. (2009). Enhanced blending elements for XFEM applied to linear elastic fracture mechanics. *77*(1), 126-148.
- Tipper, C. (1962). The brittle fracture story. Cambridge University Press, 1962. p. In.
- Ventura, G., & Benvenuti, E. J. I. J. f. N. M. i. E. (2015). Equivalent polynomials for quadrature in Heaviside function enriched elements. *102*(3-4), 688-710.

- Ventura, G., Budyn, E., & Belytschko, T. J. I. J. f. N. M. i. E. (2003). Vector level sets for description of propagating cracks in finite elements. *58*(10), 1571-1592.
- Ventura, G., Moran, B., & Belytschko, T. J. I. J. f. N. M. i. E. (2005). Dislocations by partition of unity. *62*(11), 1463-1487.
- Ventura, G. J. I. j. f. n. m. i. e. (2006). On the elimination of quadrature subcells for discontinuous functions in the extended finite-element method. *66*(5), 761-795.
- Vinh, P. C., & Malischewsky, P. G. J. U. (2006). Explanation for Malischewsky's approximate expression for the Rayleigh wave velocity. *45*(1-4), 77-81.
- Vinh, P. C., & Malischewsky, P. G. J. V. J. o. M. (2008). Improved approximations for the Rayleigh wave velocity in $[-1, 0.5]$. *30*(4), 347-358-347-358.
- Vinh, P. C., & Malischewsky, P. G. J. W. M. (2007). An approach for obtaining approximate formulas for the Rayleigh wave velocity. *44*(7-8), 549-562.
- Wells, A. (1958). The dynamic stress distribution surrounding a running crack-a photoelastic analysis. *SESA Proc.*,
- Williams, M. (1952). Stress singularities resulting from various boundary conditions in angular corners of plates in extension.
- Yoffe, E. H. J. T. L., Edinburgh,, Magazine, D. P., & Science, J. o. (1951). LXXV. The moving griffith crack. *42*(330), 739-750.
- Zi, G., Song, J.-H., Budyn, E., Lee, S.-H., Belytschko, T. J. M., Science, S. i. M., & Engineering. (2004). A method for growing multiple cracks without remeshing and its application to fatigue crack growth. *12*(5), 901.
- Zienkiewicz, O. C. J. E. E., & Dynamics, S. (1977). A new look at the Newmark, Houbolt and other time stepping formulas. A weighted residual approach. *5*(4), 413-418.